Cellular and Molecular Life Sciences (2024) 81:369
https://doi.org/10.1007/s00018-024-05408-8

ORIGINAL ARTICLE

miR-148b-5p regulates hypercalciuria and calcium-containing nephrolithiasis

Wei Zhu[1] · Zhen Zhou[1,2] · Chengjie Wu[1,3] · Zhicong Huang[1] · Ruiyue Zhao[4] · Xinlu Wang[4] · Lianmin Luo[1] · Yang Liu[1] · Wen Zhong[1] · Zhijian Zhao[1] · Guoyao Ai[1] · Jian Zhong[1] · Shusheng Liu[1] · Weijie Liu[1] · Xuliang Pang[1] · Yin Sun[1,5] · Guohua Zeng[1]

Received: 24 April 2024 / Revised: 3 August 2024 / Accepted: 11 August 2024

Abstract

Calcium-containing stones represent the most common form of kidney calculi, frequently linked to idiopathic hypercalciuria, though their precise pathogenesis remains elusive. This research aimed to elucidate the molecular mechanisms involved by employing urinary exosomal microRNAs as proxies for renal tissue analysis. Elevated *miR-148b-5p* levels were observed in exosomes derived from patients with kidney stones. Systemic administration of *miR-148b-5p* in rat models resulted in heightened urinary calcium excretion, whereas its inhibition reduced stone formation. RNA immunoprecipitation combined with deep sequencing identified *miR-148b-5p* as a suppressor of calcitonin receptor (*Calcr*) expression, thereby promoting urinary calcium excretion and stone formation. Mice deficient in *Calcr* in distal epithelial cells demonstrated elevated urinary calcium excretion and renal calcification. Mechanistically, *miR-148b-5p* regulated *Calcr* through the *circRNA-83536/miR-24-3p* signaling pathway. Human kidney tissue samples corroborated these results. In summary, *miR-148b-5p* regulates the formation of calcium-containing kidney stones via the *circRNA-83536/miR-24-3p/Calcr* axis, presenting a potential target for novel therapeutic interventions to prevent calcium nephrolithiasis.

Wei Zhu, Zhen Zhou, Chengjie Wu, and Zhicong Huang have equally contributed to this work.

✉ Guohua Zeng
gzgyzgh@vip.sina.com

[1] Department of Urology and Guangdong Key Laboratory of Urology, The First Affiliated Hospital of Guangzhou Medical University, Guangzhou 510230, Guangdong, China

[2] Department of Urology, Tianjin Institute of Urology, The Second Hospital of Tianjin Medical University, Tianjin 300211, China

[3] Department of General Surgery, Breast Center, Southern Medical University Nanfang Hospital, Guangzhou 510230, Guangdong, China

[4] Department of Nuclear Medicine, The First Affiliated Hospital of Guangzhou Medical University, Guangzhou 510230, Guangdong, China

[5] Department of Radiation Oncology, University of Rochester Medical Center, Rochester, NY 14646, USA

Published online: 25 August 2024

Graphical abstract

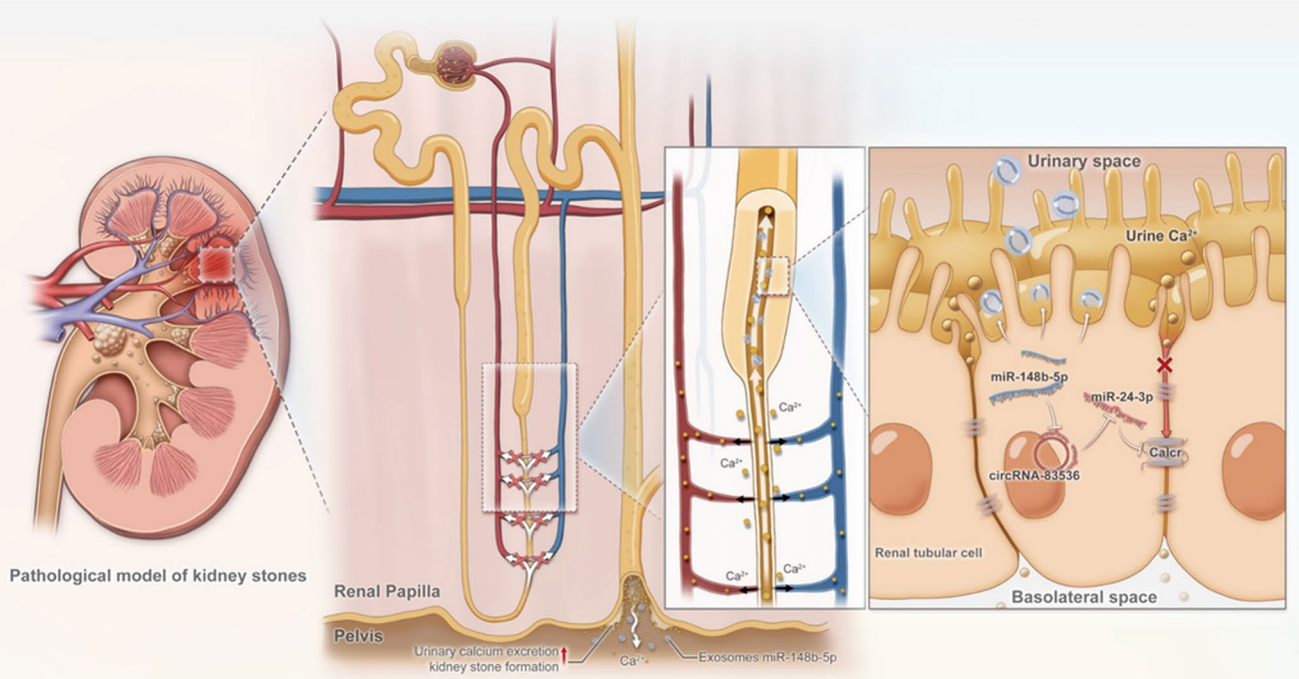

Keywords Kidney stone · Hypercalciuria · MicroRNA · Calcitonin receptor

Introduction

Kidney stone disease, or nephrolithiasis, affecting 5–10% of the global population, represents a major health concern worldwide [1, 2]. The recurrent nature of this condition poses significant challenges, as approximately 50% of patients develop subsequent kidney stones within 5 years of their initial episode [3]. Predominantly composed of calcium oxalate (CaOx) and calcium phosphate (CaP), calcium-containing kidney stones account for over 80% of all cases [4].

The formation of kidney stones is significantly influenced by various risk factors, with metabolic disturbances such as hypercalciuria, hypocitraturia, hyperoxaluria, and hyperuricosuria being particularly significant. Idiopathic hypercalciuria, marked by excessive urinary calcium excretion, is commonly observed in patients with calcium-based kidney stones [5]. The pathogenic mechanism involves the supersaturation of urinary calcium salts, leading to the precipitation and subsequent growth of crystals [4].

The initiation of kidney stone formation in patients with idiopathic hypercalciuria varies based on stone composition, yet it is primarily linked to the deposition of calcium crystals at the renal papilla, known as papillary nephrocalcinosis [6]. This deposition process is typically followed by the attachment of urinary crystals to exposed sites of interstitial CaP deposits, commonly termed Randall's plaque. These occurrences transpire after the protective urothelial layer over the renal papilla erodes. Once exposed, these sites act as anchors for the persistent deposition and growth of urinary crystals, creating a stable nidus that supports the development and gradual enlargement of kidney stones over many years [7, 8].

The etiology of idiopathic hypercalciuria remains partially elucidated. MicroRNAs, as small noncoding RNAs, regulate gene expression by binding to and either degrading or inhibiting the translation of target microRNAs. Recent studies have implicated specific miRNAs in the pathogenesis of hypercalciuria, a key risk factor for calcium kidney stones [9, 10]. Nonetheless, a significant research gap persists regarding miRNA expression profiles and their biological roles in nephrolithiasis. Expanding knowledge in this domain is imperative for a deeper comprehension of the genetic and pathophysiological mechanisms underpinning kidney stone formation.

Research on kidney stones diverges from other medical fields, such as oncology, largely due to the difficulties in acquiring adequate kidney tissue for examination. Ethical limitations typically preclude invasive techniques like renal biopsy or nephrectomy in patients with kidney stones.

Although recent methods, such as papillary biopsies, have begun illuminating the histological aspects of renal crystal deposition, these samples often lack comprehensiveness, possibly offering a constrained perspective of overall kidney pathology [11, 12]. Conversely, extracellular vesicles in biological fluids provide an easily accessible and abundant source of pathophysiological data. Extracellular miRNAs consist primarily of those actively secreted and encapsulated within exosomes and macrovesicles, along with passively released free miRNAs and those bound to RNA-binding proteins from diverse cells or tissues. The specific origins and active secretion of exosomes offer significant insights into the pathological or physiological states of the originating cells or tissues [13, 14]. Several studies have reported notable alterations in exosomal miRNA levels in the urine of patients with kidney disorders such as idiopathic nephrotic syndrome and IgA nephropathy, suggesting their potential as therapeutic targets for kidney diseases [15, 16]. However, the role of exosomal miRNAs in the pathogenesis of kidney stones remains poorly understood.

This study assessed urinary exosomal miRNA profiles in patients with calcium-containing kidney stones, identifying four miRNAs with significantly altered expression compared to healthy controls. In vitro assays and in vivo models, including rats and genetically modified mice, revealed that *miR-148b-5p*, expressed in renal tubular cells, significantly accelerated urinary calcium excretion and kidney stone formation by targeting and modulating the calcitonin receptor (*Calcr*) signaling pathway.

Materials and methods

Participants and urine sample collection

The study included 53 individuals diagnosed with CaOx kidney stones, all of whom received treatment at the Department of Urology, First Affiliated Hospital of Guangzhou Medical University (Guangzhou, China) between January and July 2019. Each patient underwent surgical stone removal, and fourier transform infrared spectroscopy confirmed the stones' chemical composition as CaOx. Exclusion criteria were defined to minimize external physical or pathological influences on urinary exosomal miRNA production. Consequently, individuals with urinary tract infections, liver or cardiovascular diseases, congenital renal or urinary abnormalities, or those under 18 years were excluded. Additionally, a control group comprising 51 healthy adults, matched for age and sex, was recruited from hospital visitors. The Ethics Committee of the First Affiliated Hospital of Guangzhou Medical University approved the study procedures, which adhered to the *Declaration of Helsinki*, and written informed consent was obtained from all participants.

Morning urine samples were collected from each participant and immediately centrifuged at 3000 g for 10 min at room temperature. Following centrifugation, the samples were stored at − 80 °C for subsequent analysis.

Urinary exosome isolation and characterization

For high-throughput Illumina sequencing by synthesis (SBS) technology, exosomes were isolated from urine samples (n = 10) of patients with CaOx kidney stones and from ten urine samples of healthy individuals. Exosome isolation employed the Ribo™ Exosome Isolation Reagent (RiboBio, Guangzhou, China), following the manufacturer's protocols. Specifically, 50 mL of urine was mixed with the isolation reagent at a 3:1 volume ratio and incubated overnight at 4 °C. The mixtures were centrifuged at 1500 g for 30 min. The resulting exosome pellets were either immediately resuspended in a minimal volume of PBS for analysis or stored at − 80 °C for future assay.

The morphology of exosomes was visualized using transmission electron microscopy (TEM, Hitachi). Exosome size distribution was analyzed with a ZETASIZER Nano series-Nano-ZS following the manufacturer's protocol. Exosomal markers CD63 and CD81 were identified via BD Accuri™ C6 flow cytometry.

MicroRNA sequencing and validation by real-time quantitative PCR (RT-qPCR)

Total RNA was isolated using TRIzol and preserved in diethylpyrocarbonate-treated water at − 20 °C. Small RNA libraries were constructed and sequenced on an Illumina HiSeq™ 2500 platform (RiboBio). For library preparation, exosomal RNA was ligated to 5' and 3' adaptors, followed by cDNA synthesis and PCR amplification. The cDNA library (18–40 nt) was purified using an acrylamide gel method. Single-end sequencing generated 50 base pair reads.

Validation of microRNA sequencing data involved a detailed examination of four specific microRNAs (*miR-31-5p*, *miR-148b-5p*, *miR-205-5p,* and *miR-574-5p*) using RT-qPCR assays on urine-derived exosomes. A 2 μg RNA aliquot extracted from exosomes was reverse transcribed with the All-in-One™ microRNA First-strand cDNA Synthesis Kit. The subsequent RT-qPCR utilized the All-in-One™ microRNA RT-qPCR Detection Kits. Relative microRNA expression levels were normalized to internal controls, namely 5S rRNA or U6 snRNA.

In silico analysis

Putative target genes of selected exosomal microRNAs were identified through computational predictions TargetScan (available at http://www.targetscan.org/mamm_31/), miRDB

(available at http://www.mirdb.org/), miRanda (available at http://www.microrna.org/microrna/home.do) and StarBase (available at http://starBase.sysu.edu.cn/). Targets confirmed by at least three databases were considered probable microRNA targets. Functional annotations of these targets were conducted using Gene Ontology (GO) and Kyoto Encyclopedia of Genes and Genomes (KEGG) pathway analyses via the DAVID 6.7 software platform. Statistical significance for identified GO terms and pathways was set at a P-value threshold of < 0.05, ensuring result reliability.

Animal studies

All rat and mouse experiments detailed herein complied with the guidelines and protocols approved by the Institutional Animal Care and Use Committee of Guangzhou Medical University.

Agomir treatment

Eight-week-old male Sprague–Dawley (SD) rats, obtained from the Guangdong Medical Laboratory Animal Center, were housed under standard conditions with ad libitum access to food and water. The experiment employed specific agomirs (RiboBio) targeting *rno-miR-31a-5p* (5′-AGG CAAGAUGCUGGCAUAGCUG-3’), *rno-miR-148b-5p* (5′-GAAGUUCUGUUAUACACUCAGG-3′), *rno-miR-205-5p* (5′-UCCUUCAUUCCACCGGAGUCUGU-3′), *hsa-miR-574-5p* (5′-UGAGUGUGUGUGUGUGAGUGUGU-3′), and a negative control (NC) agomir. These agomirs, designed as methylated and cholesterol-modified microRNA mimics for in vivo application, were prepared in sterile PBS per the manufacturer’s guidelines. Rats received weekly intraperitoneal injections of these agomirs at 30 nmol/kg body weight over 8 weeks.

Development of hypercalciuric kidney stone rat model

Eight-week-old SD rats were fed a standard chow diet containing 800 IU vitamin D3/kg and 15 g calcium/kg. The modeling method reported by Letavernier et al., with modifications, was utilized [17]. Calcium and vitamin D were selected to induce hypercalciuria and promote kidney stone formation. The rats had unrestricted access to water supplemented with 2 g/l of calcium gluconate and received intramuscular injections of vitamin D3 (100,000 IU/kg) weekly for 32 weeks. Consistent environmental enrichment strategies ensured animal welfare. Urinary compositions were assessed biweekly, with the rats housed in metabolic cages for precise urine collection and measurement.

Antagomir treatment in rats

The *rno-miR-148b-5p* antagomir (5′-CCUGAGUGUAUA ACAGAACUUC-3′) and a NC antagomir were obtained from RiboBio. Designed as an antagonist, the microRNA antagomir was modified with methylation and cholesterol for in vivo application and dissolved in autoclaved PBS following the manufacturer’s instructions. Intraperitoneal injections were administered to rats at a dose of 50 nmol/kg body weight weekly for 32 weeks.

Generation of renal tubule-specific *calcr* knockout mice and development of hypercalciuria

Generation of *Calcr* knockout mice lacking the *Calcr* gene in renal tubule cells was achieved through a breeding strategy. Mice carrying the loxP site-Calcr transgene ($Calcr^{flox/flox}$; C57BL/6 J) were mated with Cadherin 16 promoter-driven Cre (Cdh16-cre; C57BL/6 J; from Cyagen Biosciences) mice, which express the heterozygous Cre recombinase gene. This gene, regulated by the Ksp-Cdh16 promoter, is specifically expressed in renal tubule cells [18]. The floxed *Calcr* allele was engineered on a C57BL/6 J background using CRISPR-Cas9 technology (Cyagen Biosciences). Tail genotyping of the offspring followed established methods and the manufacturer's guidelines [18].

The hypercalciuria mouse model was established using a protocol similar to the rat model, involving the co-administration of calcium and vitamin D3. Eight-week-old mice had unrestricted access to water supplemented with 2 g/L calcium gluconate and received weekly intramuscular injections of vitamin D3 (200,000 IU/kg) for 32 weeks. Standard environmental enrichment practices were maintained to ensure well-being. Urinary composition was assessed biweekly by placing the mice in metabolic cages designed for precise urine collection. Additionally, monthly full-body CT scans were conducted on all mice to monitor kidney stone formation.

Antagomir treatment in $calcr^{f/f;Cdh16}$ mice

The *mmu-miR-148b-5p* antagomir (5′-AGCCUGAGUGUA UAACAGAACUUC-3′) and a NC antagomir were sourced from RiboBio. Eight-week-old mice were given unrestricted access to water supplemented with 2 g/L calcium gluconate and received intramuscular vitamin D3 injections (200,000 IU/kg) weekly for 6 weeks. The antagomir, dissolved in autoclaved PBS according to the provided protocols, was administered intraperitoneally at 120 nmol/kg body weight weekly for 6 weeks. Urinary output was

measured biweekly by housing the mice in metabolic cages to ensure precise urine collection.

Biochemical analysis of blood and urine samples

Urine oxalate and citrate concentrations were quantified via ion exchange chromatography using Metrohm (Switzerland) equipment. Calcium, phosphate, and creatinine levels in urine and serum were measured with the Unicel DxC 600 Synchron Clinical System. Additionally, pH values were determined using a glass electrode in a calibrated pH meter by Mettler Toledo (Switzerland). All analyses were performed at the Guangdong Key Laboratory of Urology, adhering to established protocols, with urine samples processed within 24 h of collection.

Quantitative assessment of renal CaOx crystal deposition

Renal CaOx crystal deposition was evaluated with Pizzolato staining, following established protocols [19]. Quantitative analysis of stained sections utilized ImageJ software.

RNA immunoprecipitation sequencing (RIP-seq)

RIP assays were conducted using a commercial RIP Kit (Bersinbio, Guangzhou, China). Rat kidney lysates were incubated with 5 µg of either an Argonaute-2 (Ago2) antibody (ab186733, Abcam) or a nonspecific anti-immunoglobulin G antibody as a control. These antibodies, bound to coated beads, were incubated overnight at 4 °C with continuous rotation. Immunoprecipitates were eluted with an elution buffer, and RNA was subsequently isolated from the eluates. This RNA was reverse-transcribed into complementary DNA (cDNA). Sequencing libraries were then prepared according to the kit's protocols and sequenced using an Illumina HiSeq™ 2500 platform (RiboBio).

Immunohistochemistry analysis (IHC)

Tissues were fixed in 10% neutral buffered formalin and embedded in paraffin. To enhance antigen exposure, antigen retrieval was performed by treating the slides with 10 mM sodium citrate (pH 6.0) at 98 °C for 20 min. Sections were then incubated with an endogenous peroxidase blocker, followed by overnight incubation at 4 °C with the primary antibody specific to *Calcr* (ab11042, Abcam) at a 1:100 dilution. After rinsing with PBS, sections were treated with a biotinylated secondary antibody for 45 min, washed, and incubated with a horseradish peroxidase (HRP)-streptavidin enzyme conjugate. Enzyme activity was visualized using DAB (Zymed, South San Francisco, CA) as the chromogen. The sections were counterstained with hematoxylin and eosin, and mounted in an aqueous medium. Immunoreactivity of renal epithelial cells was quantitatively assessed using the German immunoreactive score (IRS) system [20] (0 − 12), which multiplies the proportion of positive cells (0% = 0; 1–10% = 1; 11–50% = 2; 51–80% = 3; and 81–100% = 4) by the intensity of staining (negative = 0; weak = 1; moderate = 2; and strong = 3).

Table 1 The clinical features of controls and kidney stone patients

	C (n = 10)	P (n = 10)	P-value
Age (yrs)	50.6 ± 8.58	42.9 ± 9.23	0.077
Gender (M/F)	7/3	7/3	1
Serum creatinine (µmol/L)	79.11 ± 9.89	88.77 ± 16.45	0.129
Serum BUN (µmol/L)	4.82 ± 0.86	4.99 ± 1.16	0.713
Serum uric acid (µmol/L)	402 ± 66.43	396.1 ± 106.63	0.884
Serum calcium (µmol/L)	2.29 ± 0.16	2.32 ± 0.11	0.575
24-h urine composition			
Volume (ml)	2235 ± 665	2495 ± 883	0.467
Citrate (mg)	197.4 ± 76.09	157.3 ± 85.31	0.283
Oxalate (mg)	36.1 ± 15.3	51.2 ± 13.84	0.033
Calcium (mmol)	2.91 ± 1.37	7.27 ± 2.32	< 0.001
Phosphate (mmol)	12.86 ± 4.27	20.44 ± 3.98	0.001
Creatinine (mmol)	12.25 ± 2.68	13.68 ± 2.63	0.24
Urate (mmol)	2.59 ± 0.90	3.68 ± 0.88	0.014
Sodium (mmol)	138.02 ± 30.77	172.21 ± 48.16	0.075
Potassium (mmol)	38.14 ± 9.88	45.24 ± 17.57	0.28
Magnesium (mmol)	3.23 ± 0.86	3.79 ± 1.81	0.389
pH	6 ± 0.41	6.4 ± 0.46	0.054

Fluorescence in situ hybridization (FISH)

FISH targeting specific microRNAs and circular RNAs (circRNAs) was conducted on paraffin-embedded kidney tissue sections following established protocols [3]. Oligonucleotide probes designed to hybridize with *miR-148b-5p*, *miR-24-3p*, and the junction site of *circRNA-83536*, along with a Tissue Pretreatment FISH kit, were sourced from Exonbio Lab (Guangzhou, China). Probe sequences included: 5′-GCCTGAGTGTATAACAGAACTT-3′ (*hsa-miR-148b-5p*), 5′-CCTGAGTGTATAACAGAACTTC-3′ (*rno-miR-148b-5p*), 5′-AGAATCTAAGAATGCCTCTTG CACTG-3′ (*hsa-circRNA-83536*), and 5′-CTGTTCCTG CTGAACTGAGCCA-3′ (*hsa/rno-miR-24-3p*). Each probe was end-labelled with digoxigenin (DIG) at both 5′ and 3′ ends and incorporated 2′-fluoro-modified RNA residues for enhanced thermal stability. Kidney sections, 10 µm thick, were deparaffinized and dehydrated, then treated with 0.2 M HCl for 15 min. Slides were subsequently immersed in PBS and treated with Proteinase K (200 µg/ml in PBS) at 37 °C for 5 min to improve probe penetration. Following enzymatic

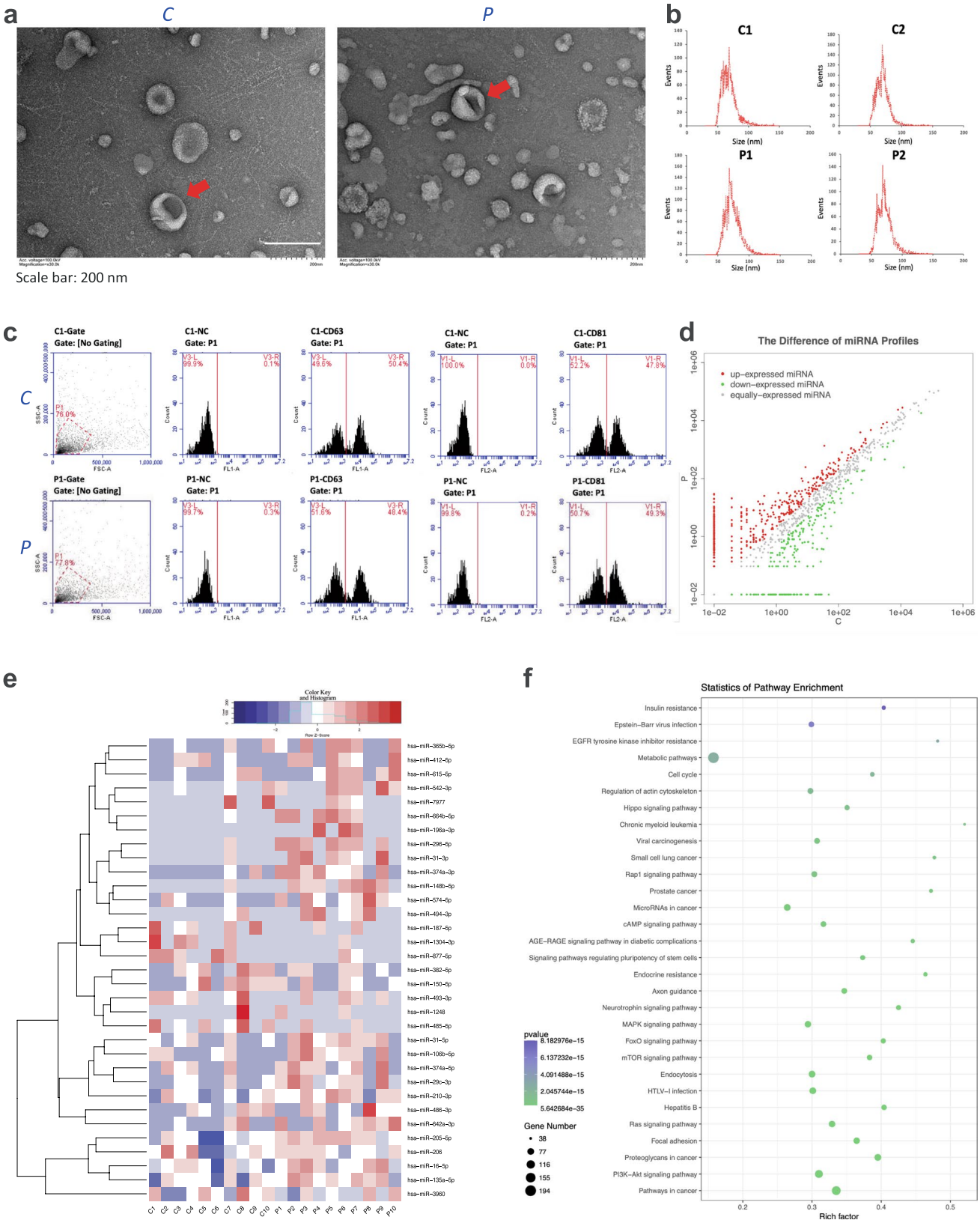
a
C
P
Scale bar: 200 nm
b
C1
C2
P1
P2
Events
Size (nm)
c
C1-Gate
Gate: [No Gating]
C1-NC
Gate: P1
C1-CD63
Gate: P1
C1-NC
Gate: P1
C1-CD81
Gate: P1
P1-Gate
Gate: [No Gating]
P1-NC
Gate: P1
P1-CD63
Gate: P1
P1-NC
Gate: P1
P1-CD81
Gate: P1
SSC-A
FSC-A
Count
d
The Difference of miRNA Profiles
up−expressed miRNA
down−expressed miRNA
equally−expressed miRNA
P
C
e
Color Key and Histogram
Row Z-Score
hsa−miR−365b−5p
hsa−miR−412−5p
hsa−miR−615−5p
hsa−miR−542−3p
hsa−miR−7977
hsa−miR−664b−5p
hsa−miR−196a−3p
hsa−miR−298−5p
hsa−miR−31−3p
hsa−miR−374a−3p
hsa−miR−148b−5p
hsa−miR−574−5p
hsa−miR−494−3p
hsa−miR−187−5p
hsa−miR−1304−3p
hsa−miR−877−5p
hsa−miR−382−5p
hsa−miR−150−5p
hsa−miR−493−3p
hsa−miR−1248
hsa−miR−485−5p
hsa−miR−31−5p
hsa−miR−106b−5p
hsa−miR−374a−5p
hsa−miR−29c−3p
hsa−miR−210−3p
hsa−miR−486−3p
hsa−miR−642a−3p
hsa−miR−205−5p
hsa−miR−206
hsa−miR−16−5p
hsa−miR−135a−5p
hsa−miR−3960
C1 C2 C3 C4 C5 C6 C7 C8 C9 C10 P1 P2 P3 P4 P5 P6 P7 P8 P9 P10
f
Statistics of Pathway Enrichment
Insulin resistance
Epstein−Barr virus infection
EGFR tyrosine kinase inhibitor resistance
Metabolic pathways
Cell cycle
Regulation of actin cytoskeleton
Hippo signaling pathway
Chronic myeloid leukemia
Viral carcinogenesis
Small cell lung cancer
Rap1 signaling pathway
Prostate cancer
MicroRNAs in cancer
cAMP signaling pathway
AGE−RAGE signaling pathway in diabetic complications
Signaling pathways regulating pluripotency of stem cells
Endocrine resistance
Axon guidance
Neurotrophin signaling pathway
MAPK signaling pathway
FoxO signaling pathway
mTOR signaling pathway
Endocytosis
HTLV−I infection
Hepatitis B
Ras signaling pathway
Focal adhesion
Proteoglycans in cancer
PI3K−Akt signaling pathway
Pathways in cancer
pvalue
8.182976e−15
6.137232e−15
4.091488e−15
2.045744e−15
5.642684e−35
Gene Number
38
77
116
155
194
Rich factor

◂**Fig. 1** Differential expression of urine exosomal microRNAs in CaOx kidney stone patients compared to controls. **a** The morphology and structure of urinary exosomes observed under TEM, with exosomes displaying typical characteristics indicated by red arrows. **b** The size distribution of exosomes from both control and kidney stone patient groups, analyzed via Zetasizer Nano-ZS. **c** Detection of exosomal markers CD63 and CD81 through flow cytometry. **d** Volcano plots depicting the microRNA expression profiles between control and kidney stone patient groups. **e** Heatmap visualizing the differentially expressed exosomal microRNAs, with red indicating high relative expression and green indicating low relative expression. **f** KEGG pathway enrichment bubble plot for differentially expressed microRNAs between the groups. C represents the control group, and P denotes the CaOx kidney stone patient group, with n = 10 for each group

treatment, the slides were rinsed in RNase-free water for 5 min and air-dried. Prehybridization occurred at 37 °C for 2 h in a hybridization buffer, followed by hybridization with specific oligonucleotide probes at the same temperature for 48 h. Post-hybridization, the slides were washed twice with 2 × SSC and 0.5% Tween-20 for 5 min each at room temperature to eliminate non-specific binding. microRNA and circRNA visualization employed an anti-DIG antibody conjugated with HRP, with signal amplification via TSA fluorescence. Nuclear counterstaining was conducted using DAPI (1 mg/mL). Images were captured using a fluorescence microscope and quantitatively analyzed with ImageJ software.

Culture and maintenance of cell lines

Cell lines, including HK-2 (human proximal tubular), HEK-293 T (human embryonic kidney), 209/MDCT (mouse distal convoluted tubule), and mlMCD-3 (mouse collecting duct), were sourced from the American Type Culture Collection (ATCC, USA). Cultured in DMEM supplemented with 10% FBS and 1% penicillin/streptomycin, these cell lines were maintained to ensure optimal growth and viability.

Plasmid construction, RNA interference, and transfection procedures

Custom-designed short hairpin RNAs (shRNAs), along with microRNA mimics and inhibitors, were produced by RiboBio. The microRNA inhibitors featured 2'-O-methyl modifications to enhance stability and binding affinity. For *circRNA-83536* overexpression, its sequence was amplified and subcloned into the pCE-RB-Mam-NeoR vector (RiboBio). Knockdown of *circRNA-83536* was achieved by constructing a plasmid using the pRNAT-U6.1/Neo vector (RiboBio). Transfection of these constructs into cells was conducted using Lipofectamine 3000 reagent according to Invitrogen's protocol (Carlsbad, CA, USA). Details of the shRNA target sequence against *circRNA-83536* are provided in Supplementary Table 2.

Table 2 The expression of *miR-31-5p*, *miR-148b-5p*, *miR-205-5p* and *miR-574-5p* confirmed with RT-qPCR in urinary exosomes from controls and patients with kidney stones in the screening phase and the validation set. (The expression levels were normalized to the expression of 5S rRNA.)

miRNAs	Screening phase				Validation set			
	Controls (n = 10)	Patients (n = 10)	log2(fold change P vs. C)	P value	Controls (n = 41)	Patients (n = 43)	log2(fold change P vs. C)	P value
miR-31-5p	8.689	247.651	4.833	0.001	3.445	152.661	5.470	< 0.001
miR-148b-5p	1.157	31.692	4.776	0.015	2.341	43.399	4.212	< 0.001
miR-205-5p	256.333	1129.572	2.139	0.016	31.544	423.662	3.747	< 0.001
miR-574-5p	2.844	26.271	3.207	0.032	4.112	31.098	2.919	< 0.001

Table 3 The results of Spearman's rank correlations between 4 candidates urinary exosomal miRNAs and 24-h urine compositions

miRNAs	Urine calcium	Urine oxalate	Urine citrate	Urine urate	Urine phosphate
miR-31-5p	0.559 P = 0.01	0.339 P = 0.144	0.071 P = 0.767	0.482 P = 0.031	0.641 P = 0.002
miR-148b-5p	0.640 P = 0.002	0.311 P = 0.182	− 0.031 P = 0.897	0.378 P = 0.1	0.439 P = 0.053
miR-205-5p	0.529 P = 0.017	0.221 P = 0.35	-0.311 P = 0.183	0.258 P = 0.272	0.536 P = 0.015
miR-574-5p	0.705 P = 0.001	0.446 P = 0.049	-0.206 P = 0.384	0.505 P = 0.023	0.449 P = 0.047

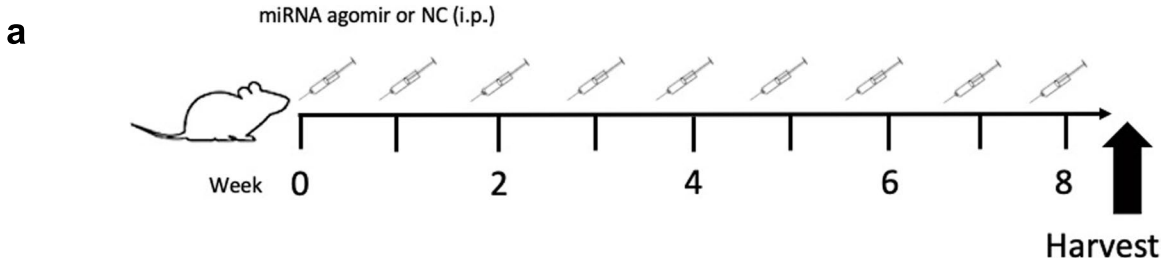
a
miRNA agomir or NC (i.p.)
Week 0 2 4 6 8
Harvest

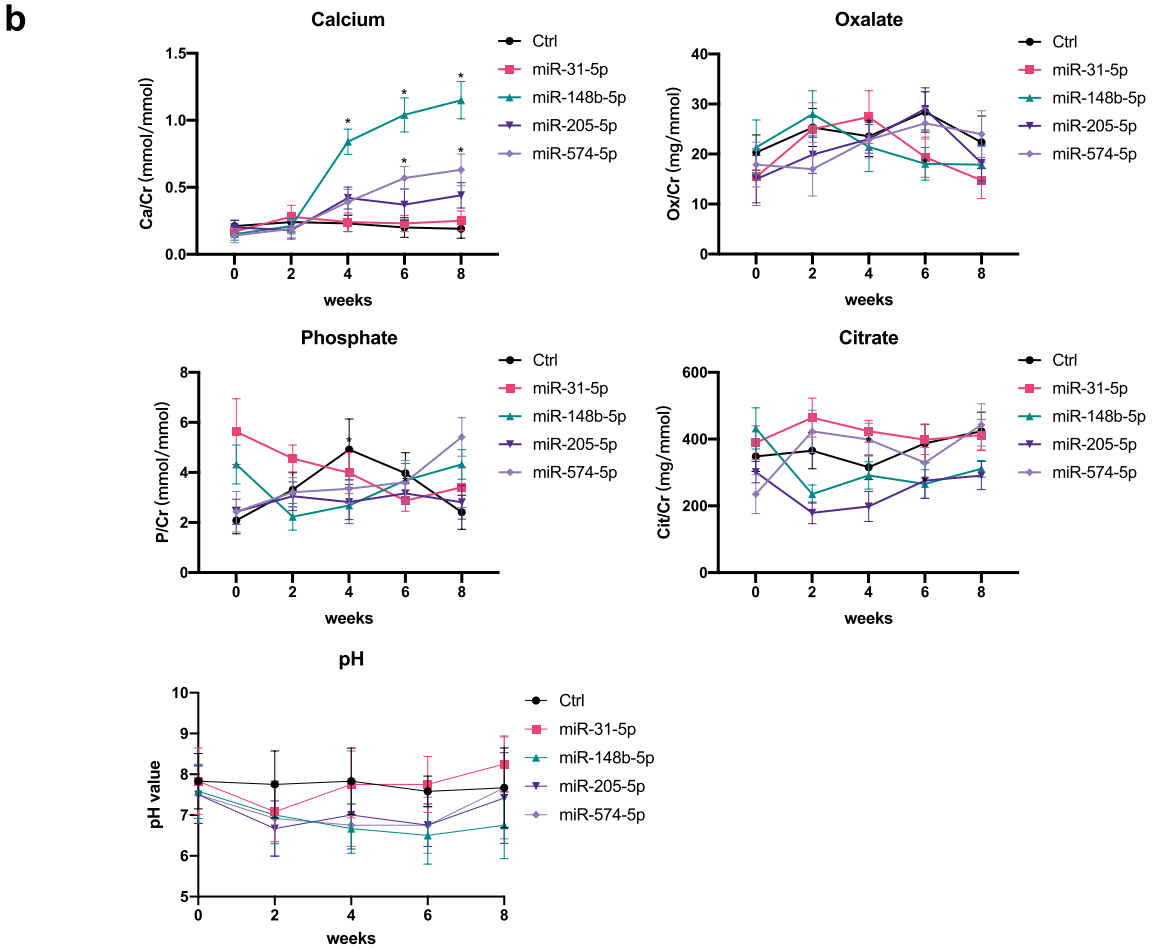
b
Calcium
Ca/Cr (mmol/mmol)
weeks
Oxalate
Ox/Cr (mg/mmol)
weeks
Phosphate
P/Cr (mmol/mmol)
weeks
Citrate
Cit/Cr (mg/mmol)
weeks
pH
pH value
weeks
Ctrl
miR-31-5p
miR-148b-5p
miR-205-5p
miR-574-5p

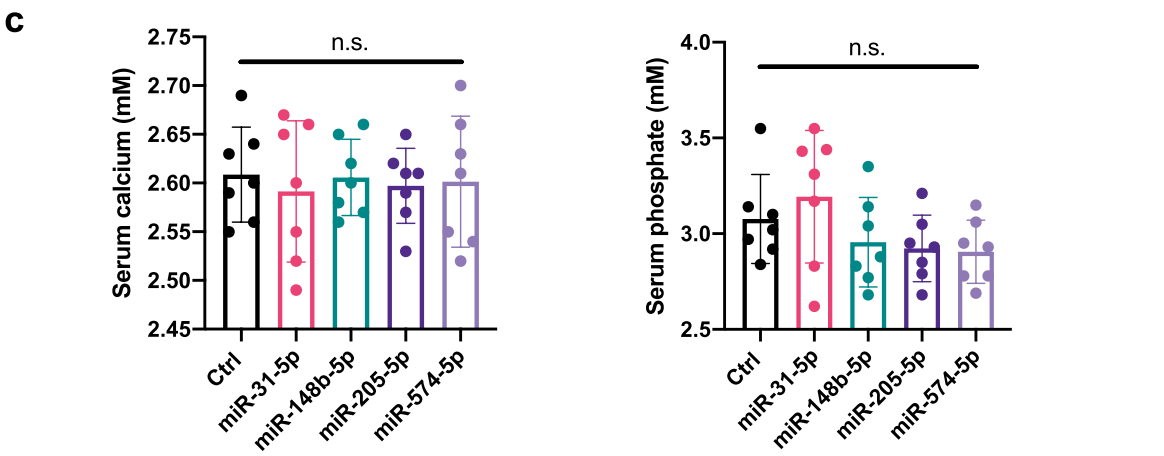
c
Serum calcium (mM)
n.s.
Serum phosphate (mM)
n.s.
Ctrl
miR-31-5p
miR-148b-5p
miR-205-5p
miR-574-5p

◂**Fig. 2** *MiR-148b-5p* agomir treatment increased urinary calcium excretion in rats. **a** Schematic of the intraperitoneal injection schedule for microRNA agomir. **b** Measurements of 24-h urinary calcium, oxalate, phosphate, citrate excretion, and urine pH at 0, 2, 4, 6, and 8 weeks post-treatment. **c** Serum calcium and phosphate concentrations in rats. NC denotes negative control (Ctrl group). Data are presented as mean ± SD from 7 rats per group. n.s indicates not significant; $*P < 0.05$ compared to control group (Student's t-test)

Gene expression quantification

Total RNA was extracted from the samples using TRIzol reagent, following the manufacturer's standardized protocols (Invitrogen). RNA was reverse-transcribed into cDNA with the PrimeScript RT reagent Kit (Takara, China). RT-qPCR assays were performed on a Bio-Rad CFX96 system using SYBR Green (Takara) to quantify mRNA expression. Relative expression levels of the target gene were normalized to glyceraldehyde-3-phosphate dehydrogenase (GAPDH) mRNA as an internal control. Primer sequences used in this analysis are listed in Supplementary Table 3.

Western blot assay

Protein analysis was performed by lysing cells in RIPA buffer, followed by electrophoretic separation of 10–50 μg of total protein extracts using a 10% SDS-PAGE system. Separated proteins were electro-transferred onto PVDF membranes, which were subsequently blocked with a 5% non-fat milk solution in TBST to prevent non-specific binding. Membranes were incubated with primary antibodies specific to *Calcr* (ab11042, Abcam) at a 1:1000 dilution and then exposed to HRP-conjugated secondary antibodies. Protein bands were visualized using the ECL detection system from Thermo Fisher Scientific (Waltham, MA). The intensity of the bands was quantitatively analyzed using ImageJ software by subtracting background noise.

The mRNA-microRNA pull-down assay

Collected cell lysates with 1.5 μl of RNase inhibitor were combined with 500 pmol/L biotin-labeled antisense oligos targeting *Calcr* mRNA (5′-CTGGAAATGAATCAGAGA GTGCAT-3′) and rotated overnight at 4 °C. Biotin-labeled antisense oligos against green fluorescent protein mRNA (5′-ATAGATGAACTTCAGGCAGTCCTT-3′) served as a NC. Following the addition of 10 μL Streptavidin Agarose beads, the lysate mixture was rotated for 2 h at 4 °C. The mixture was then centrifuged at 3000 rpm for 2 min, and the beads were washed five times with cell lysis buffer. Total RNA was extracted using TRIzol (Invitrogen) per the manufacturer's protocol. After reverse transcription, RT-qPCR analysis detected *miR-148b-5p* or *miR-24-3p* pulled down by *Calcr*. U6 snRNA was used as an internal control.

RNase resistance assay

Total RNA was isolated using TRIzol lysis followed by PureLink purification targeting the aqueous phase. Each 1 μg RNA sample was treated with 20 U RNase R (Epicenter) or underwent a mock treatment in a 10 μL reaction volume containing 1 × RNase R buffer and 1 U/μL ribonuclease inhibitor (New England Biolabs) at 37 °C for 1 h. The reaction mixture was then supplemented with 1 μL of 1 mM EDTA, 1 μL of 10 mM dNTP, and 1 μL of 100 M random hexamers, denatured at 65 °C for 5 min, and cooled on ice. For cDNA synthesis, 4 μL of 10 × buffer (125 mM KCl, 250 mM Tris–HCl/pH 8.0, 15 mM $MgCl_2$), 1 μL murine ribonuclease inhibitor (40 U/μL), and 1 μL Superscript III (Life Technologies) were added, with incubation steps at 25 °C for 10 min, 50 °C for 50 min, 55 °C for 10 min, and 85 °C for 5 min, followed by cooling to 4 °C. A 1 μL aliquot of this cDNA was then used as a template for quantitative RT-PCR analysis.

Luciferase reporter assay

A fragment of the human *Calcr* 3'untranslated region (3'UTR) containing two *miR-24-3p* binding sites was amplified by PCR using forward primer 5′-CAGTAATTC TAGGCGATCGCCGAGGAGAGTGCTGAGAT-3′ and reverse primer 5′-GATATTTTATTGCGGCCAGCTTTT CTCTGGGTGCGCTA-3′. These 3'UTRs were cloned into the psiCHECK™ reporter vector (Promega, USA) via the Gibson assembly method. HEK293T cells were co-transfected with 25 ng of luciferase constructs [wild-type (WT) or mutant 3'UTR] and 20 nmol of *miR-24-3p* mimics or a control mimic (Ctrl). After 48 h, luciferase activity was measured using the Dual-luciferase Reporter Assay System (Promega) in accordance with the manufacturer's protocol.

RNA antisense purification (RAP) assay

The RAP assay utilized a RAP Kit (Axl-bio, Guangzhou, China). Initially, 1×10^8 cells underwent cross-linking to preserve endogenous RNA complexes, which were then captured with biotinylated antisense oligonucleotides specific to the target sequence. Streptavidin-coated beads were prepared for RAP and NC groups with the designated number of probes (probe sequence: ACAGCTGCAGAGTCG AAGAATCTAAGAATGCCTCCTGCACTGCAATGT CCATTGGGCTG). Rigorous washing steps minimized non-specific RNA interactions. RNA directly interacting with *circRNA-83536* was extracted using TRIzol reagent, reverse transcribed, and analyzed for binding efficiency by RT-qPCR. Specific sequences of *circRNA-83536* for human, mouse, and rat, including binding sites for *miR-24-3p* and *miR-148b-5p*, were detailed in Supplementary Fig. 4.

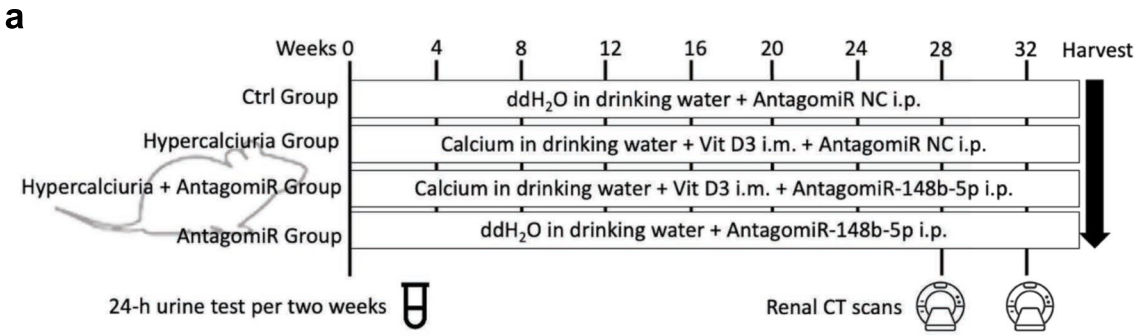

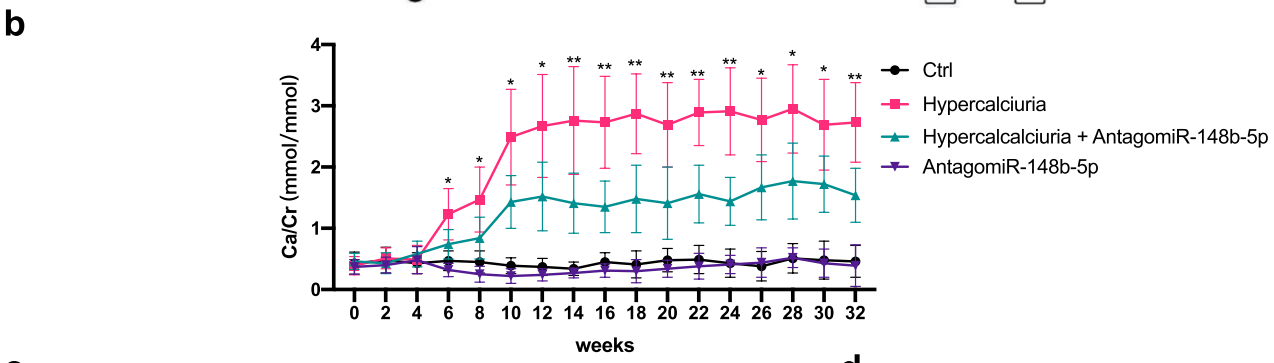

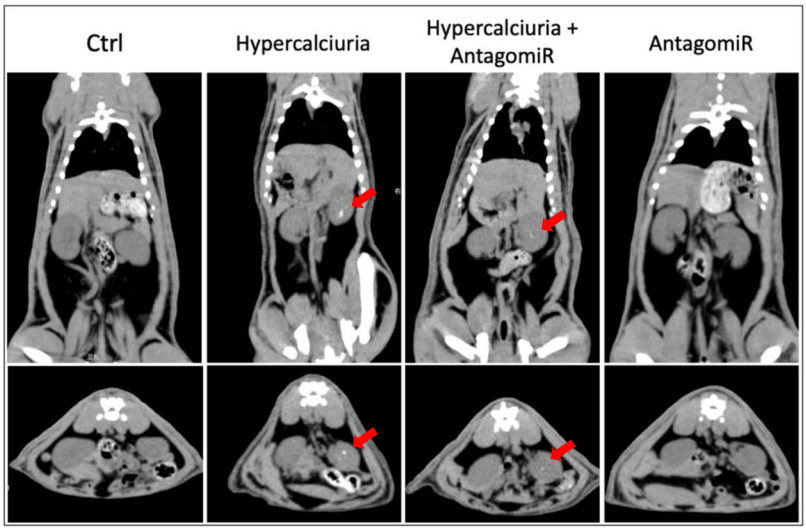

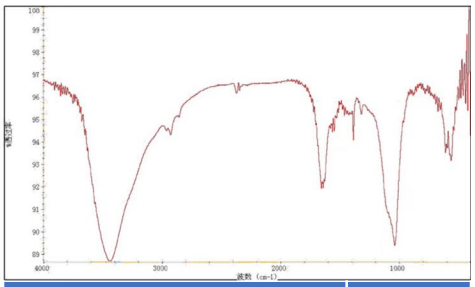

Component	Content
Calcium phosphate	43%
Carbonate-apatite	37%
Calcium oxalate	12%
Matrix (usually protein)	8%

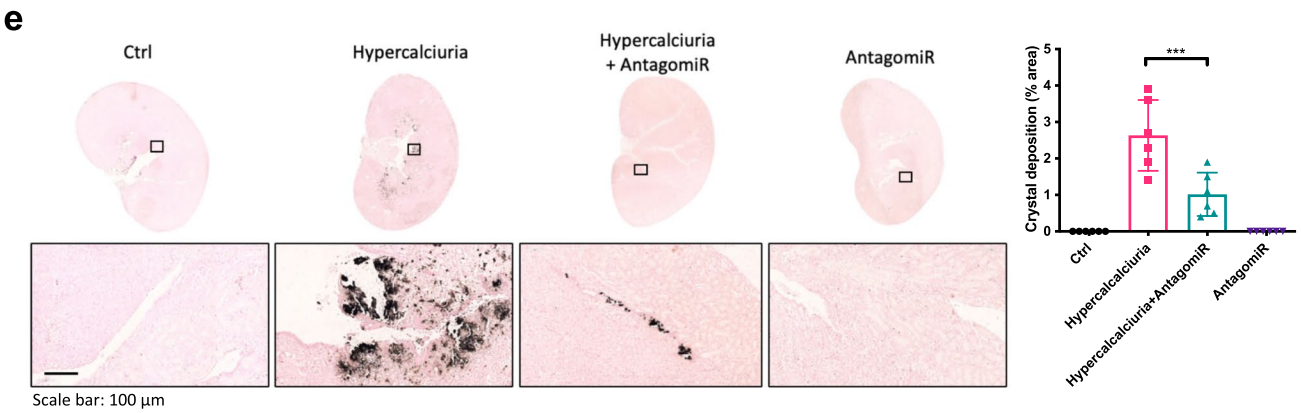

◂**Fig. 3** Administration of *miR-148b-5p* antagomir reduced urinary calcium excretion and kidney stone formation in a hypercalciuria rat model. **a** Schematic representation of the induction of hypercalciuria in rats and the intraperitoneal injection protocol for microRNA antagomir. **b** Measurement of 24-h urinary calcium excretion in various rat groups. **c** CT scan analysis of kidney stone formation across the rat groups, with red arrows indicating the presence of kidney stones. **d** Kidney stone composition, identified as a mixture of CaP, carbonate-apatite, and CaOx, determined through Fourier-transform infrared spectroscopy. **e** Pizzolato staining showing crystal deposition in the renal papilla and its quantification (right panel). Data are presented as mean ± SD, with 6 rats per group. Statistical significance is indicated as follows: n.s., not significant; *P < 0.05, **P < 0.01, ***P < 0.001 compared to the hypercalciuria group (One-Way ANOVA test)

Collection of human kidney tissue samples

Human kidney tissue samples were obtained from normal kidney tissue areas during radical nephrectomy for renal cell carcinoma or from renal papillae tissues during nephrectomy for non-functioning kidneys caused by kidney stones. All samples were collected from the First Affiliated Hospital of Guangzhou Medical University with patient consent. The Institutional Ethics Committee approved the study involving human subjects.

Statistical analysis

Statistical analyses were performed using SPSS software, version 18.00. Continuous variables were analyzed with one-way ANOVA and Student's t-tests to evaluate differences among groups. Categorical variables, expressed as frequencies and percentages, were assessed using chi-square or Fisher's exact tests based on data distribution and sample size. A two-sided P-value of less than 0.05 was considered statistically significant.

Results

Differential expression of microRNAs in urinary exosomes from patients with CaOx kidney stones

This case–control study aimed to elucidate the urinary exosomal microRNA profiles unique to patients with CaOx kidney stones. Utilizing Illumina SBS technology, the expression levels of over 2000 microRNAs were quantified in 20 urine samples, comprising specimens from 10 controls and 10 patients with CaOx kidney stones. Comparative analyses revealed no significant differences in demographic or baseline clinical parameters, including age, sex, renal function (measured by serum creatinine and blood urea nitrogen), serum uric acid, and calcium levels among the participants. However, individuals with CaOx kidney stones exhibited significantly higher urinary excretion of calcium, oxalate, urate, and phosphate (Table 1).

Validating the efficiency and purity of the exosome extraction process was essential before analyzing exosomal microRNAs. Exosomes extracted from urine samples were first visualized via TEM, revealing the characteristic round morphology with membrane-bound structures typical of exosomes (Fig. 1a). Subsequent Zetasizer Nano-ZS analysis confirmed their size range between 50 and 100 nm in diameter (Fig. 1b). Flow cytometry further verified the purity and identity of the isolated exosomes, which prominently expressed CD63 and CD81 [21] (Fig. 1c), confirming the successful extraction of urine exosomes.

Differential expression of urinary exosomal microRNAs between kidney stone patients and healthy controls was visualized using volcano plots and heatmaps (Fig. 1d-e). Hierarchical clustering analysis identified 819 differentially expressed microRNAs out of 2588 analyzed (523 upregulated and 296 downregulated) (Supplementary Table 1). Target prediction for microRNAs with $\log_2$(fold change) ≥ 1 and P-value < 0.05 was conducted using miRDB, miRWalk, TargetScan, and miRTarBase. Subsequent KEGG pathway analysis of predicted target genes revealed associations with key signaling pathways, including metabolic pathways, MAPK signaling, Rap1 signaling, and cAMP signaling (Fig. 1f). Understanding these pathways is essential for elucidating the pathophysiology of kidney stone formation and the molecular mechanisms involved.

Subsequently, we selected microRNAs with significant differences between the two groups guided by criteria including a p-value below 0.05, a fold change exceeding 2, and relatively uniform expression levels across all samples within each group (Table 2). Spearman's rank correlation test assessed the relationships between these microRNAs and 24-h urine profiles indicative of kidney stone pathogenesis. The analysis identified four microRNAs (*miR-31-5p*, *miR-148b-5p*, *miR-205-5p*, *miR-574-5p*) with strong positive correlations to urinary concentrations of calcium, oxalate, urate, and phosphate, which are instrumental in stone formation (Table 3). Consequently, these four microRNAs were chosen for further investigation to elucidate their roles in kidney stone formation.

RT-qPCR assays validated microRNA profiles in additional independent cohorts, comprising 41 controls and 43 patients with CaOx kidney stones. Results were consistent with initial Illumina SBS data, revealing significantly elevated levels of four specific microRNAs in the urine of patients with CaOx kidney stones compared to controls (Table 2).

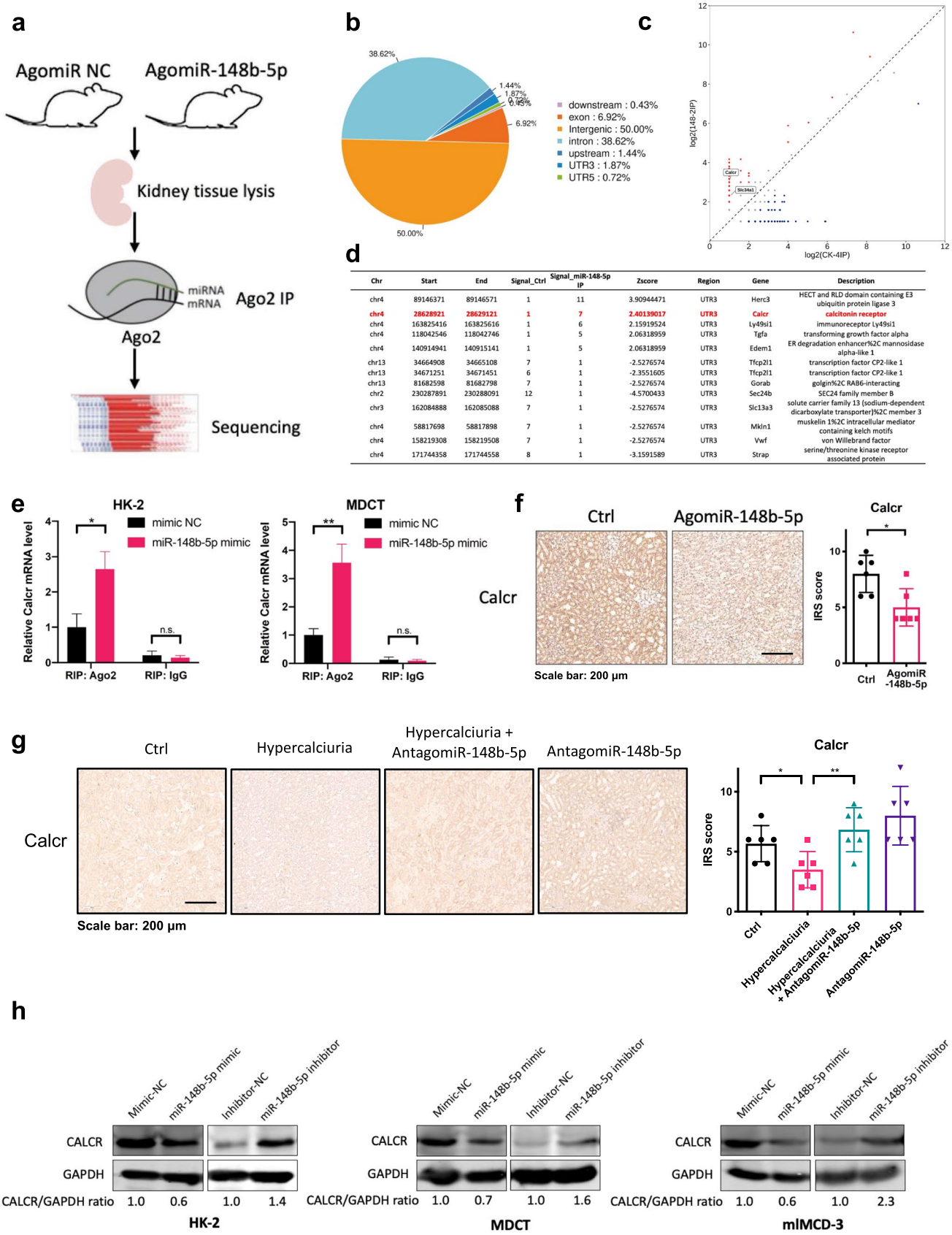
a
AgomiR NC
AgomiR-148b-5p
Kidney tissue lysis
miRNA
mRNA
Ago2 IP
Ago2
Sequencing
b
38.62%
1.44%
1.87%
0.72%
6.92%
50.00%
downstream : 0.43%
exon : 6.92%
Intergenic : 50.00%
intron : 38.62%
upstream : 1.44%
UTR3 : 1.87%
UTR5 : 0.72%
c
log2(148-2IP)
log2(CK-4IP)
Calcr
Slc34a1
d
Chr Start End Signal_Ctrl Signal_miR-148-5p IP Zscore Region Gene Description
chr4 89146371 89146571 1 11 3.90944471 UTR3 Herc3 HECT and RLD domain containing E3 ubiquitin protein ligase 3
chr4 28628921 28629121 1 7 2.40139017 UTR3 Calcr calcitonin receptor
chr4 163825416 163825616 1 6 2.15919524 UTR3 Ly49si1 immunoreceptor Ly49si1
chr4 118042546 118042746 1 5 2.06318959 UTR3 Tgfa transforming growth factor alpha
chr4 140914941 140915141 1 5 2.06318959 UTR3 Edem1 ER degradation enhancer%2C mannosidase alpha-like 1
chr13 34664908 34665108 7 1 -2.5276574 UTR3 Tfcp2l1 transcription factor CP2-like 1
chr13 34671251 34671451 6 1 -2.3551605 UTR3 Tfcp2l1 transcription factor CP2-like 1
chr13 81682598 81682798 7 1 -2.5276574 UTR3 Gorab golgin%2C RAB6-interacting
chr2 230287891 230288091 12 1 -4.5700433 UTR3 Sec24b SEC24 family member B
chr3 162084888 162085088 7 1 -2.5276574 UTR3 Slc13a3 solute carrier family 13 (sodium-dependent dicarboxylate transporter)%2C member 3
chr4 58817698 58817898 7 1 -2.5276574 UTR3 Mkln1 muskelin 1%2C intracellular mediator containing kelch motifs
chr4 158219308 158219508 7 1 -2.5276574 UTR3 Vwf von Willebrand factor
chr4 171744358 171744558 8 1 -3.1591589 UTR3 Strap serine/threonine kinase receptor associated protein
e
HK-2
mimic NC
miR-148b-5p mimic
Relative Calcr mRNA level
RIP: Ago2
RIP: IgG
n.s.
MDCT
f
Ctrl
AgomiR-148b-5p
Calcr
Scale bar: 200 μm
IRS score
g
Ctrl
Hypercalciuria
Hypercalciuria + AntagomiR-148b-5p
AntagomiR-148b-5p
Calcr
Scale bar: 200 μm
IRS score
Hypercalciuria + AntagomiR-148b-5p
h
Mimic-NC
miR-148b-5p mimic
Inhibitor-NC
miR-148b-5p inhibitor
CALCR
GAPDH
CALCR/GAPDH ratio 1.0 0.6 1.0 1.4
HK-2
CALCR/GAPDH ratio 1.0 0.7 1.0 1.6
MDCT
CALCR/GAPDH ratio 1.0 0.6 1.0 2.3
mIMCD-3

◂**Fig. 4** *MiR-148b-5p* enhanced urinary calcium excretion by downregulating *Calcr* expression. **a** Workflow of Ago2 RIP-seq experiments in rat kidney tissue treated with *miR-148b-5p* agomir or NC agomir. **b** Pie chart illustrating the distribution of significant Ago2 peaks in various genomic regions: upstream, 5' UTR, intron, exon, intergenic, 3' UTR, and downstream. **c** Scatter plots displaying Ago2 peak profiles in kidney tissues from *miR-148b-5p* agomir and control groups. **d** Differential Ago2 RIP-seq identified 13 putative mRNA 3'UTRs predicted to interact with *miR-148b-5p*. **e** Ago2 RIP in HK-2 and MDCT cells transfected with *miR-148b-5p* mimics (50 nM) for 48 h, compared to mock-transfected cells. **f** IHC staining of *Calcr* in kidney tissues from rats treated with *miR-148b-5p* agomir or NC agomir (6 samples per group). **g** IHC staining of *Calcr* in kidney tissues from hypercalciuria rats treated with or without *miR-148b-5p* antagomir (6 samples per group). **h** *Calcr* expression levels 48 h after transfection with *miR-148b-5p* mimics (50 nM) or antisense inhibitor (100 nM) in HK-2, MDCT, and mlMCD-3 cells. Data are presented as mean ± SD. n.s., not significant; $*P < 0.05$, $**P < 0.01$ (Student's t-test)

These results confirmed the upregulation of four urinary exosomal microRNAs in patients with CaOx kidney stones. Additionally, these microRNAs showed a significant positive correlation with urinary compositions involved in kidney stone pathogenesis.

Systemic delivery of *miR-148b-5p* agomir increases urinary calcium excretion in rats

The functional role of four urinary exosomal microRNAs in kidney stone pathogenesis was investigated by systemically administering corresponding agomirs to rats and evaluating alterations in urinary components linked to kidney stone formation (detailed in Fig. 2a). Administration of agomirs targeting *miR-148b-5p* and *miR-574-5p* significantly elevated urinary calcium excretion without notably affecting other urinary components associated with kidney stone pathophysiology, such as oxalate, phosphate, pH, and citrate (Fig. 2b). Additionally, these treatments did not alter serum calcium and phosphate concentrations (Fig. 2c).

The data in Fig. 2a-c indicated that *miR-148b-5p* and *miR-574-5p* enhance urinary calcium excretion, suggesting their roles as critical factors in the risk profile for calcium-containing kidney stone development. Given its greater impact on increasing urinary calcium excretion compared to *miR-574-5p*, *miR-148b-5p* was selected for more detailed subsequent experiments.

Systemic delivery of *miR-148b-5p* antagomir suppresses kidney stone formation by diminishing urinary calcium excretion in a rat model

The functional role of *miR-148b-5p* in pathogenesis was assessed in a rat model that mimicked human kidney stone formation through co-administration of vitamin D3 and a high-calcium diet. This regimen induces hypercalciuria, renal Randall's plaque formation, and CaP or CaOx stones, paralleling human conditions [17]. Hypercalciuric rats received intraperitoneal injections of chemically modified antisense oligonucleotides targeting *miR-148b-5p*, while the control group was treated with a scramble sequence antagomir (detailed in Fig. 3a). The 24-h urinary compositions were monitored biweekly. Treatment with the *miR-148b-5p* antagomir significantly reduced urinary calcium excretion (Fig. 3b) and markedly suppressed the formation of Randall's plaque and kidney stones after a 32-week regimen of vitamin D3 and high-calcium intake (Fig. 3c-e).

These in vivo results (Fig. 3a-e) demonstrated that inhibiting *miR-148b-5p* with antagomir significantly mitigated kidney stone formation by primarily reducing urinary calcium excretion.

Mechanistic insights of *miR-148b-5p* in increasing urinary calcium excretion Via downregulation of *Calcr* expression

A detailed approach using Ago2 RNA immunoprecipitation followed by deep sequencing (Ago2 RIP-Seq) elucidated the molecular mechanisms of *miR-148b-5p* in accelerating urinary calcium excretion. Ago2, a crucial component of the RNA-induced silencing complex (RISC), binds microRNA and its mRNA targets [22]. Kidney tissues from rats treated with *miR-148b-5p* agomir or NC agomir were lysed, and Ago2 was immunoprecipitated using specific antibodies. RNA extracted from these immunoprecipitates was subjected to high-throughput sequencing to identify microRNA-mRNA interactions (Fig. 4a). Following Ago2 RIP-Seq, 694 putative differentially expressed microRNAs were identified. Among these, 13 microRNAs with Ago2 binding sites in their 3'UTRs exhibited the most significant differential expression post-agomir treatment (Fig. 4b-d). To refine our search for potential mRNA targets of *miR-148b-5p* involved in the modulation of urinary calcium excretion, our focus was narrowed to transporter genes known for their roles in the regulation of calcium or other ions and demonstrated increases in Ago2 binding activity. The candidate gene, *Calcr*, a G protein-coupled receptor essential for maintaining calcium homeostasis and known to be involved in kidney stones pathogenesis in humans [33], emerged as a key candidate for further investigation.

In *vitro* studies using cell lines further substantiated the findings. Parallel Ago2 RIPs were conducted on renal tubular cells (HK-2 and MDCT), transfected with *miR-148b-5p* mimics, and compared to mock-transfected controls. These assays revealed a significant increase in Ago2 binding to *Calcr* mRNA in *miR-148b-5p*-transfected cells relative to mock-transfected cells (Fig. 4e).

To directly evaluate the impact of *miR-148b-5p* on *Calcr* expression, IHC was performed on kidney sections

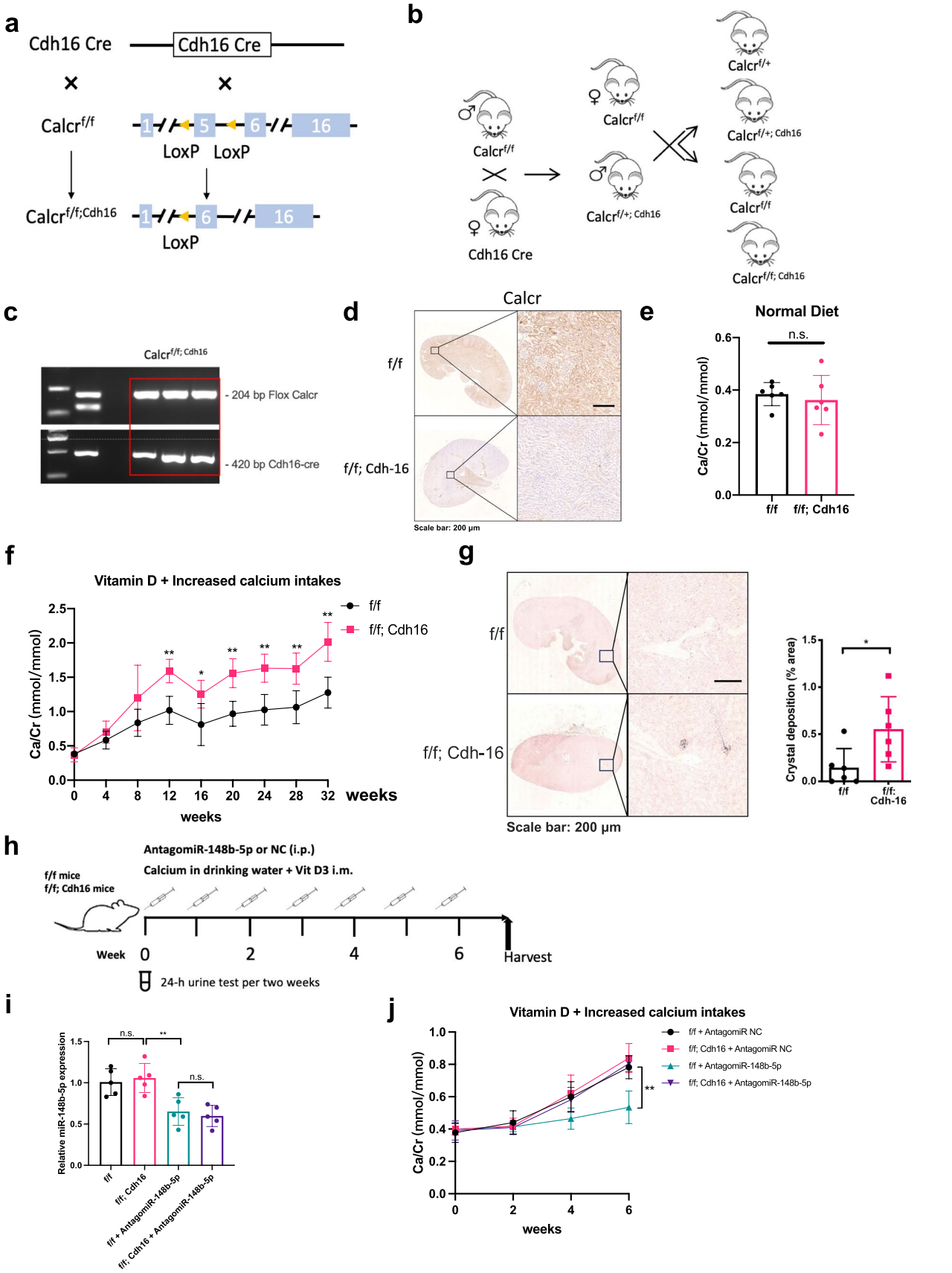
a
Cdh16 Cre
Cdh16 Cre
Calcr f/f
1 5 6 16
LoxP LoxP
Calcr f/f;Cdh16
1 6 16
LoxP
b
Calcr f/f
Cdh16 Cre
Calcr f/f
Calcr f/+; Cdh16
Calcr f/+
Calcr f/+; Cdh16
Calcr f/f
Calcr f/f; Cdh16
c
Calcr f/f; Cdh16
- 204 bp Flox Calcr
- 420 bp Cdh16-cre
d
Calcr
f/f
f/f; Cdh-16
Scale bar: 200 μm
e
Normal Diet
n.s.
Ca/Cr (mmol/mmol)
f/f
f/f; Cdh16
f
Vitamin D + Increased calcium intakes
f/f
f/f; Cdh16
Ca/Cr (mmol/mmol)
weeks
g
f/f
f/f; Cdh-16
Scale bar: 200 μm
Crystal deposition (% area)
f/f
f/f: Cdh-16
h
AntagomiR-148b-5p or NC (i.p.)
Calcium in drinking water + Vit D3 i.m.
f/f mice
f/f; Cdh16 mice
Week 0 2 4 6
Harvest
24-h urine test per two weeks
i
Relative miR-148b-5p expression
n.s.
**
n.s.
f/f
f/f; Cdh16
f/f + AntagomiR-148b-5p
f/f; Cdh16 + AntagomiR-148b-5p
j
Vitamin D + Increased calcium intakes
f/f + AntagomiR NC
f/f; Cdh16 + AntagomiR NC
f/f + AntagomiR-148b-5p
f/f; Cdh16 + AntagomiR-148b-5p
Ca/Cr (mmol/mmol)
weeks

◂**Fig. 5** Renal tubular epithelial *Calcr* gene loss increased urinary calcium excretion and CaOx crystal deposition in mice administered vitamin D and increased calcium intake. **a** Protocol for preparing $Calcr^{f/f;\ Cdh16}$ mice. **b** Breeding scheme for $Calcr^{f/f;\ Cdh16}$ mice. **c** Tail genomic DNA isolation for PCR genotyping. (**d**) IHC analysis of *Calcr* protein expression in kidneys of $Calcr^{f/f}$ and $Calcr^{f/f;\ Cdh16}$ mice. (**e**) Comparison of 24-h urinary calcium excretion between $Calcr^{f/f}$ and $Calcr^{f/f;\ Cdh16}$ mice under a normal diet. (**f**) Comparison of 24-h urinary calcium excretion between $Calcr^{f/f}$ and $Calcr^{f/f;\ Cdh16}$ mice after co-administration of vitamin D3 and increased calcium intake. (**g**) Comparison of renal CaOx crystal deposition between $Calcr^{f/f}$ and $Calcr^{f/f;\ Cdh16}$ mice after 32 weeks of vitamin D3 co-administration and increased calcium intake. (**h**) Diagram of the hypercalciuria mouse model development and i.p. injection schedule for microRNA agomir. (**i**) RT-qPCR analysis of *miR-148b-5p* expression in kidney tissues from hypercalciuria mice induced by vitamin D3 and increased calcium intake, treated with *miR-148b-5p* antagomir. Expression levels were normalized to U6 snRNA. (**j**) Comparison of 24-h urinary calcium excretion between $Calcr^{f/f}$ and $Calcr^{f/f;\ Cdh16}$ mice treated with *miR-148b-5p* antagomir. Data are presented as mean ± SD from 6 mice per group. n.s indicates not significant; $^{*}P < 0.05$, $^{**}P < 0.01$ (Student's t-test)

from rats treated with *miR-148b-5p* agomir or antagomir. Results indicated a downregulation of *Calcr* expression in rats receiving *miR-148b-5p* agomir (Fig. 4f), while an upregulation *Calcr* was noted in hypercalciuria rats treated with *miR-148b-5p* antagomir (Fig. 4g). Additionally, transfection of *miR-148b-5p* mimics into renal tubular cells (HK-2, MDCT, and mlMCD-3) suppressed *Calcr* expression at the protein level (Fig. 4h) but not at the mRNA level (Supplementary Fig. 1). Conversely, transfection with the *miR-148b-5p* antisense inhibitor into renal tubular cells increased Calcr expression at the protein level (Fig. 4h), without affecting the mRNA level (Supplementary Fig. 1).

Overall, the data from Fig. 4a-h and Supplementary Fig. 1 suggested that *miR-148b-5p* potentially increased urinary calcium excretion by diminishing *Calcr* protein expression.

In vivo studies to determine the role of *Calcr* in calcium-containing kidney stones formation using genetically modified mice

To elucidate the functional impact of the *Calcr* on urinary calcium excretion and kidney stone formation, renal tubule-specific *Calcr* knockout mice were generated by crossbreeding floxed *Calcr* mice with Cdh16 promoter-driven Cre recombinase mice, restricting Cre activity to renal tubule segments, including Bowman's capsule, proximal tubules, the loop of Henlé, and distal tubule [18] (Fig. 5a-b). Genotyping confirmed the successful generation of $Calcr^{f/f;Cdh16}$ mice by examining Cre and floxed *Calcr* alleles (Fig. 5c). Effective deletion of *Calcr* in the renal tubules of $Calcr^{f/f;Cdh16}$ mice was validated at the protein level via IHC, which showed a marked decrease in *Calcr* expression compared to control $Calcr^{f/f}$ mice (Fig. 5d).

Urinary calcium excretion in $Calcr^{f/f;Cdh16}$ mice was analyzed to determine the functional consequences of *Calcr* deletion. Under normal dietary conditions, urinary calcium levels in $Calcr^{f/f;Cdh16}$ mice were similar to those in $Calcr^{f/f}$ control mice (Fig. 5e). However, co-administration of vitamin D and increased calcium intake led to a significantly higher increase in urinary calcium excretion in $Calcr^{f/f;Cdh16}$ mice compared to $Calcr^{f/f}$ mice (Fig. 5f). This was further supported by more pronounced tubular calcifications in the renal papilla of $Calcr^{f/f;Cdh16}$ mice after 32 weeks of co-administration of vitamin D and increased calcium intake, compared to $Calcr^{f/f}$ mice (Fig. 5g).

The kidney-specific knockout of *Calcr* provides a critical test to determine whether exogenous *miR-148b-5p* affects urinary calcium regulation through non-renal organs with systemic delivery. To investigate this, the impact of *miR-148b-5p* antagomir on urinary calcium excretion was assessed in a mouse model co-administered with vitamin D and increased calcium intake. Results indicated that a 6-week injection of the *miR-148b-5p* antagonist reduced urine calcium levels only in $Calcr^{f/f}$ mice, but not in $Calcr^{f/f;Cdh16}$ mice (Fig. 5h-j).

These results (Fig. 5a-j) suggested that *Calcr* knockout in renal epithelial cells correlated with increased urinary calcium excretion and renal tubular calcifications. Additionally, the regulation of urine calcium by exogenous *miR-148b-5p* appears to depend on renal *Calcr* expression.

Mechanistic insights of *miR-148b-5p* in suppressing *Calcr* protein expression by downregulating *circRNA-83536*

To elucidate the molecular mechanism by which *miR-148b-5p* reduces *Calcr* expression, a fragment from the *Calcr* 3'UTR was inserted into the psiCHECK™-2 dual-luciferase reporter vector downstream of the Renilla luciferase gene. Luciferase assays demonstrated significant suppression of luciferase activity by *miR-148b-5p* in constructs containing the *Calcr* 3'UTR (Fig. 6a). However, no predicted microRNA-responsive elements within the *Calcr* 3'UTR matched the seed sequence of *miR-148b-5p*. Additionally, a mRNA pull-down assay in renal tubular cells showed no direct interaction between *miR-148b-5p* and *Calcr* mRNA (Fig. 6b). These results suggested that *miR-148b-5p* likely targeted the *Calcr* 3'UTR indirectly to modulate its expression.

To investigate the mechanisms mediating the suppression of *Calcr* expression by *miR-148-5p*, the potential involvement of circRNAs was examined. CircRNAs are known to function as microRNA sponges, regulating microRNA activity within cells [23]. It was hypothesized that *miR-148b-5p*

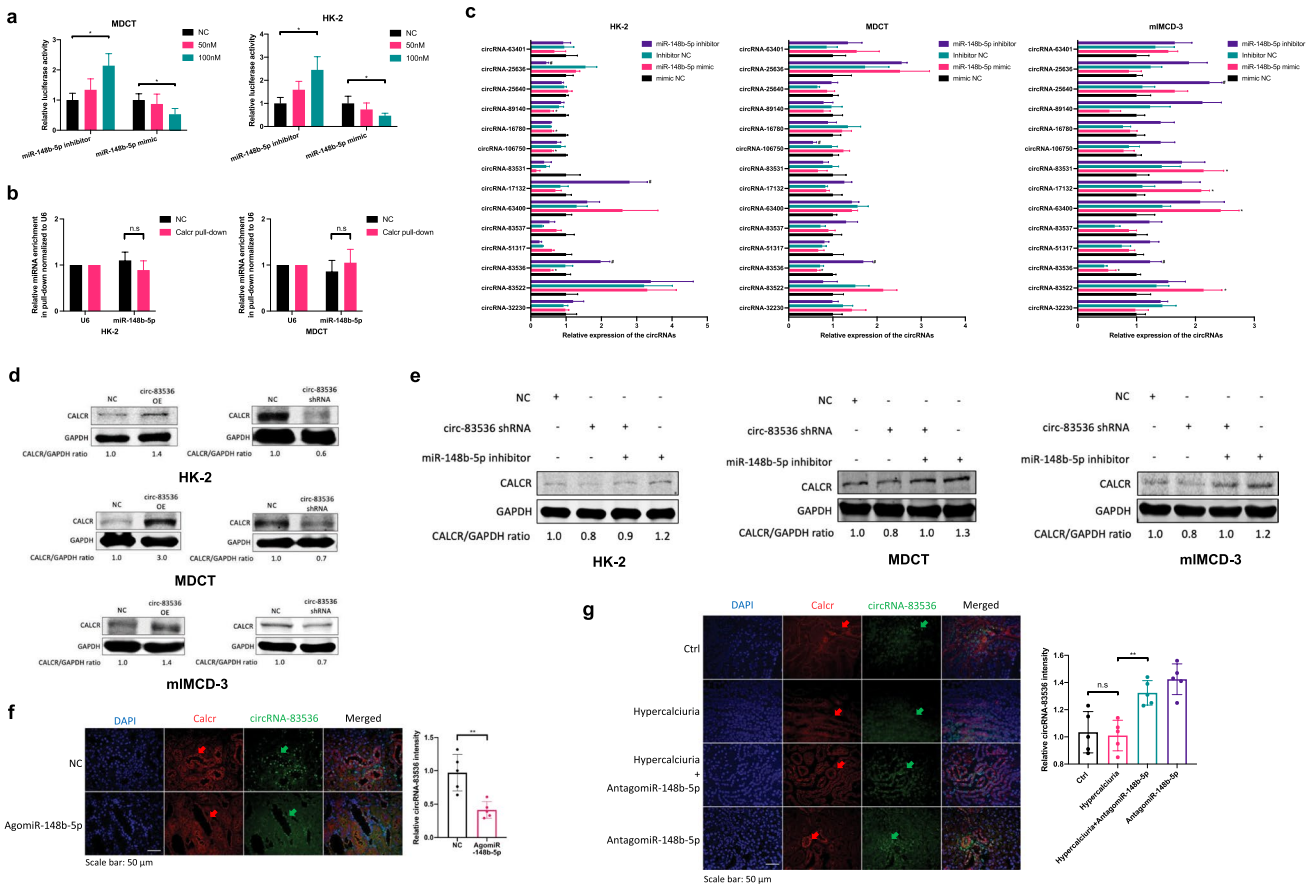

Fig. 6 *MiR-148b-5p* modulates Calcr via downregulation of *circRNA-83536*. **a** Co-transfection of the *Calcr* 3'UTR construct with *miR-148b-5p* mimics or antisense inhibitor into HK-2 and MDCT cells, followed by luciferase assay to measure activity. **b** RNA pull-down assay revealed that *Calcr* does not bind to *miR-148b-5p* in HK-2 and MDCK cells. **c** Screening of potential circular RNA candidates modulated by *miR-148b-5p* using RT-qPCR in HK-2, MDCT, and mlMCD-3 cells. Transfection was performed with *miR-148b-5p* mimics (50 nM) or antisense inhibitor (100 nM) for 24 h, with expression levels normalized to GAPDH. $^{*}P<0.05$ compared to mimic NC group, $^{\#}P<0.05$ compared to inhibitor NC group. **d** Western blot analysis showed that shRNA-mediated knockdown of *circRNA-83536* (250 ng/ml) reduced *Calcr* protein expression, while overexpression of *circRNA-83536* (250 ng/ml) increased *Calcr* it in HK-2, MDCT, and mlMCD-3 cells. **e** Transduction of *circRNA-83536* shRNA (250 ng/ml) into HK-2, MDCT, and mlMCD-3 cells reversed the *Calcr* protein increase induced by *miR-148b-5p* inhibition (100 nM), as demonstrated by Western blot. **f** FISH and IF images showing *circRNA-83536* (green arrows) and *Calcr* (red arrows) expression in kidney tissues from rats treated with *miR-148b-5p* agomir. **g** FISH and IF images detecting *circRNA-83536* (green arrows) and *Calcr* (red arrows) expression in kidney tissues from hypercalciuria rats induced by vitamin D3 and increased calcium intake treated with *miR-148b-5p* antagomir. Data are presented as mean ± SD, with 5 rats per group. n.s., not significant; $^{*}P<0.05$ (Student's t-test)

repression could alter the expression of specific circRNAs, thus releasing other microRNAs and subsequently restricting *Calcr* expression. Database analyses (RNA22 [24], Circular RNA Interactome [25], and circAtlas [26]) identified 14 circRNAs as potential *miR-148b-5p* targets that might influence *Calcr* expression through microRNA sequestration. RT-qPCR analysis was performed to validate whether any of these circRNAs were targets of *miR-148b-5p* in renal tubular cells. Results revealed a significant downregulation of *hsa_circ_0083536* (*circRNA-83536*), derived from the human *XPO7* gene, following *miR-148b-5p* overexpression in renal tubular cells, and an increase upon *miR-148b-5p* inhibition with a specific antisense inhibitor (Fig. 6c).

The effects of *circRNA-83536* on *Calcr* expression were further investigated by knocking down or overexpressing *circRNA-83536* in renal tubular cells. Alterations in *circRNA-83536* levels significantly influenced *Calcr* expression (Fig. 6d). Specifically, targeted knockdown of *circRNA-83536* with shRNA partially counteracted the *miR-148b-5p*-induced suppression of *Calcr* expression in renal tubular cells (Fig. 6e). The effectiveness of *circRNA-83536* overexpression and knockdown was validated through RT-qPCR in renal tubular cells (Supplementary Fig. 2a-b).

Additionally, the stability and circular nature of *circRNA-83536* were confirmed using an RNase R digestion assay. Unlike linear GAPDH mRNA, which was

substantially reduced by RNase R, circRNA-83536 remained intact, verifying its circular form in HK-2 cells (Supplementary Fig. 2c).

Further investigations using RNA FISH and co-immunofluorescence (IF) staining revealed that *miR-148b-5p* agomir treatment significantly reduced *circRNA-83538* and *Calcr* expression in rat renal tissues (Fig. 6f). Conversely, administration of *miR-148b-5p* antagomir reversed these effects (Fig. 6g).

These data collectively suggested that *miR-148b-5p* decreased *Calcr* protein expression by downregulating *circRNA-83536*.

Mechanistic insights of *circRNA-83536* in orchestrating *Calcr* expression Via *miR-24-3p* downregulation

To elucidate the molecular mechanisms by which *circRNA-83536* alters *Calcr* expression, the potential of circRNAs to function as microRNA sponges, a role increasingly recognized for its significance in disease progression, was considered [27].

Venn analysis identified microRNAs potentially mediating this regulation by targeting the 3'UTR of *Calcr* and binding to *circRNA-83536*. In silico analyses using CircInteractome and miRanda databases, along with existing literature, revealed that *circRNA-83536* potentially interacted with six microRNAs targeting the 3′UTR of *Calcr* (Fig. 7a).

The RAP assay further delineated the interaction of *circRNA-83536* with these six candidate microRNAs. This experiment confirmed the direct binding of *miR-24-3p* to *circRNA-83536* in MDCT cells (Fig. 7b). Subsequent investigations into the regulatory effects of *miR-24-3p* on *Calcr* involved transfecting renal tubular cells (HK-2, MDCT, and mlMCD-3) with *miR-24-3p* mimics or antisense inhibitors. Results confirmed that *miR-24-3p* constrained *Calcr* expression (Fig. 7c). Notably, inhibition of *miR-24-3p* counteracted the reduction in *Calcr* protein levels induced by sh*circRNA-83536* (Fig. 7d).

FISH analysis revealed that *miR-148b-5p* agomir treatment in rats significantly increased *miR-24-3p* expression and reduced renal *Calcr* signals (Fig. 7e) (Supplementary Fig. 3a). Conversely, treatment with *miR-148b-5p* antagomir in hypercalcinuria rat models elevated renal *Calcr* expression while decreasing *miR-24-3p* signals (Fig. 7f) (Supplementary Fig. 3c). Expression levels of *circRNA-83536*, *miR-24-3p*, and *Calcr* mRNA in kidney tissues were assessed using RT-qPCR. Results indicated decreased renal *circRNA-83536* and increased *miR-24-3p* in rats treated with *miR-148b-5p* agomir, with no significant change in *Calcr* mRNA levels (Supplementary Fig. 3b). In contrast, treatment with *miR-148b-5p* antagomir in hypercalciuria rat models led to decreased renal *miR-24-3p* and elevated *circRNA-83536* expression (Supplementary Fig. 3d).

To validate the suppressive effect of *miR-24-3p* on *Calcr* expression, RNA pull-down was performed to assess the binding of *miR-24-3p* to *Calcr* mRNA. The results indicated significantly higher expression of *miR-24-3p* in the pull-down of *Calcr* mRNA (Fig. 7g). Potential binding sites for *miR-24-3p* were identified in the 3'UTR of *Calcr* mRNA. A luciferase reporter system containing the *Calcr* 3'UTR was engineered using the psiCHECK™-2 vector, along with a mutant version at the predicted target sites. Luciferase assays demonstrated that *miR-24-3p* curtailed luciferase activity driven by the wild-type *Calcr* 3'UTR but had no effect on the mutant construct, confirming the direct targeting of the *Calcr* 3'UTR by *miR-24-3p* (Fig. 7h).

Results from Fig. 7a-h and Supplementary Fig. 3a-d suggested that *circRNA-83536* may function by sequestering *miR-24-3p* to modulate *Calcr* expression.

Correlations among *miR-148b-5p, circRNA-83536, miR-24-3p,* and *Calcr* in clinical kidney samples

To determine if the mechanisms identified in animal models and cell cultures are applicable to humans, the expression levels of *miR-148b-5p*, *circRNA-83536*, *miR-24-3p*, and *Calcr* were examined in kidney tissues from 8 CaOx kidney stone patients and 8 non-stone formers. Non-stone formers' tissue samples were sourced from normal kidney tissues during radical nephrectomy for renal cell carcinoma, whereas samples from kidney stone patients were obtained from nephrectomy due to chronic pain in a poorly functioning renal unit. IHC staining revealed weaker *Calcr* signals in CaOx kidney stone patients compared to non-stone formers (Fig. 8a). Additionally, FISH and IF assays indicated higher expression levels of *miR-148b-5p* and *miR-24-3p*, alongside lower expression levels of *circRNA-83536* and Calcr in kidney tissues from CaOx kidney stone patients (Fig. 8b-c).

Overall, data from Fig. 8a-c corroborated that elevated *miR-148b-5p* levels in kidney stone patients were associated with reduced expression of *circRNA-83536* and *Calcr*, reinforcing a negative correlation between *Calcr* and *miR-24-3p* expression in human kidney tissues.

Discussion

Hypercalciuria is the primary risk factor for calcium-containing kidney stone development, significantly impacting calcium transport within the kidney. This study demonstrates that *miR-148b-5p* significantly influences calcium stone formation by enhancing urinary calcium excretion through the suppression of *circRNA-83536/miR-24-3p/Calcr* signaling (Fig. 9). These results provide valuable insights into

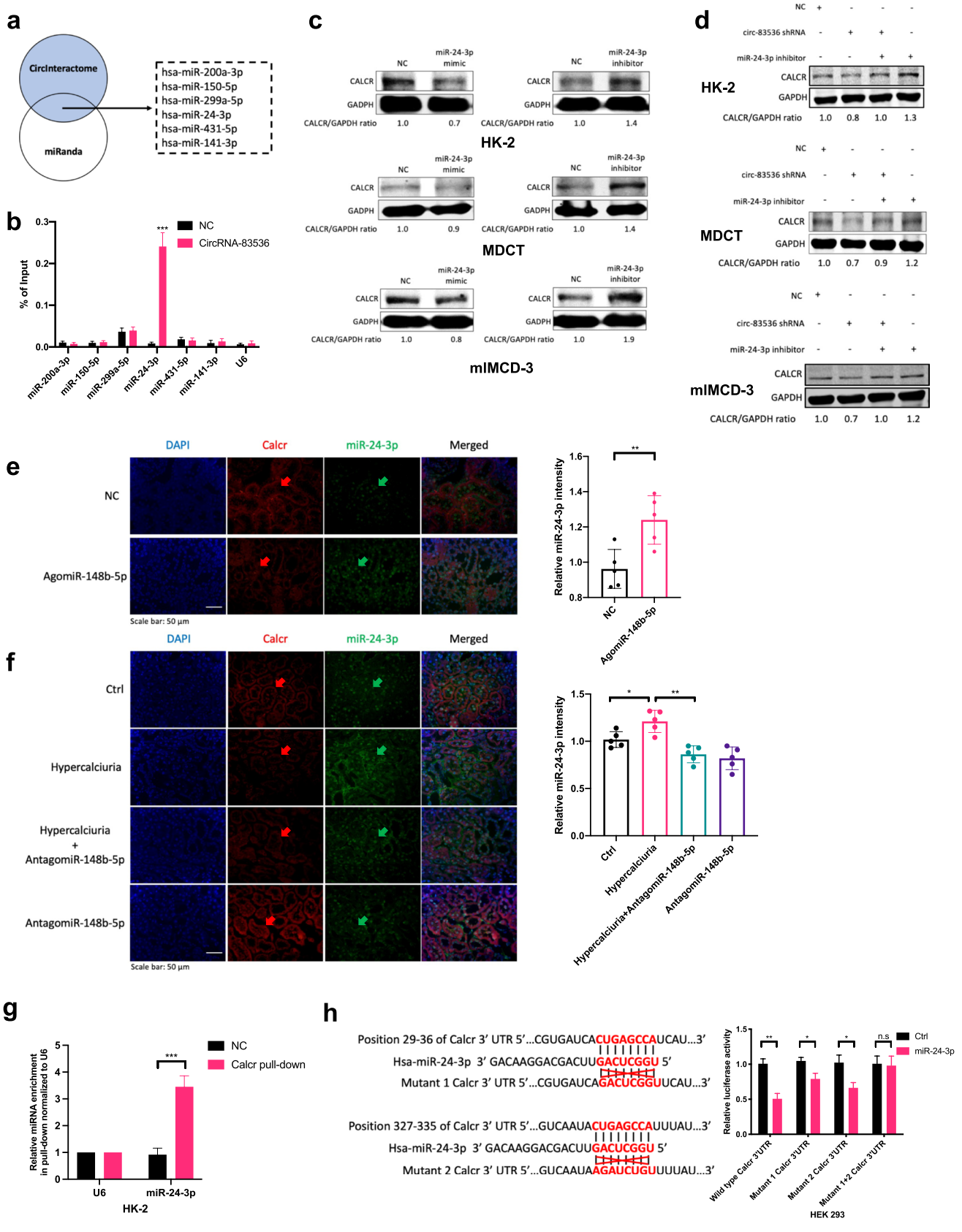
a
CircInteractome
miRanda
hsa-miR-200a-3p
hsa-miR-150-5p
hsa-miR-299a-5p
hsa-miR-24-3p
hsa-miR-431-5p
hsa-miR-141-3p
b
% of Input
NC
CircRNA-83536
miR-200a-3p
miR-150-5p
miR-299a-5p
miR-24-3p
miR-431-5p
miR-141-3p
U6
c
NC
miR-24-3p mimic
miR-24-3p inhibitor
CALCR
GADPH
CALCR/GADPH ratio
HK-2
MDCT
mIMCD-3
d
circ-83536 shRNA
miR-24-3p inhibitor
e
DAPI
Calcr
miR-24-3p
Merged
AgomiR-148b-5p
Scale bar: 50 μm
Relative miR-24-3p intensity
f
Ctrl
Hypercalciuria
Hypercalciuria + AntagomiR-148b-5p
AntagomiR-148b-5p
g
Relative miRNA enrichment in pull-down normalized to U6
Calcr pull-down
h
Position 29-36 of Calcr 3′ UTR 5′...CGUGAUCACUGAGCCAUCAU...3′
Hsa-miR-24-3p 3′ GACAAGGACGACUUGACUCGGU 5′
Mutant 1 Calcr 3′ UTR 5′...CGUGAUCAGACUCGGUUCAU...3′
Position 327-335 of Calcr 3′ UTR 5′...GUCAAUACUGAGCCAUUUAU...3′
Hsa-miR-24-3p 3′ GACAAGGACGACUUGACUCGGU 5′
Mutant 2 Calcr 3′ UTR 5′...GUCAAUAAGAUCUGUUUUAU...3′
Relative luciferase activity
Wild type Calcr 3'UTR
Mutant 1 Calcr 3'UTR
Mutant 2 Calcr 3'UTR
Mutant 1+2 Calcr 3'UTR
HEK 293

◂**Fig. 7** *CircRNA-83536* modulated *Calcr* expression by downregulating *miR-24-3p*. **a** Venn plot identifying six microRNAs potentially regulated by *circRNA-83536*, which can bind to both *Calcr* and *circRNA-83536*. **b** RAP assay for the binding of *circRNA-83536* to six miRNAs (predicted by online database) in MDCT cells. The results confirmed the binding of *miR-24-3p* with *circRNA-83536* in MDCT cells. **c** Transducing the *miR-24-3p* mimics (50 nM) into renal tubular cells for 48 h suppressed *Calcr* expression, while transducing the *miR-24-3p* inhibitor (100 nM) for 48 h increased Calcr expression. **d** Transducing the *miR-24-3p* inhibitor (100 nM) into renal tubular cells for 48 h reversed Calcr protein expression by sh*circRNA-83536* (250 ng/ml), as shown by Western blot. **e** Representative FISH images displaying *Calcr* (red arrows) and *miR-24-3p* (green arrows) expression in kidney tissues from rats treated with *miR-148b-5p* agomir (5 samples per group). **f** Representative IF images showing *Calcr* (red arrows) and *miR-24-3p* (green arrows) expression in kidney tissues from hypercalciuria rats induced by vitamin D3 and high calcium intake, treated with *miR-148b-5p* antagomir (5 samples per group). **g** RNA pull-down assay demonstrating the binding of *Calcr* to *miR-24-3p* in HK-2 cells. **h** Co-transfection of *Calcr* 3'-UTR constructs containing wild-type or mutant 1 and mutant 2 seed regions with *miR-24-3p* into HEK-293T cells, followed by a luciferase assay to measure luciferase activity. Data are presented as mean ± SD. n.s., not significant; $^{*}P < 0.05$, $^{**}P < 0.01$, $^{***}P < 0.001$ (Student's t-test)

potential strategies for modulating *miR-148b-5p*-mediated signaling to prevent calcium-containing kidney stones. Additionally, *miR-148b-5p* shows promise as a biomarker for dysregulation in *Calcr* signaling, contributing to increased urinary calcium excretion.

Analyzing human tissue samples is often the initial step in understanding the molecular basis of diseases, but such samples are difficult to procure for benign conditions compared to malignant diseases like tumors. An alternative involves analyzing urinary exosomes, secreted by all nephron segments and containing an RNA profile similar to renal tissue [15, 28]. Urinary exosomes exhibit notable enrichment and integrity of microRNAs compared to cell-free urine, making them a valuable source for disease research and biomarker discovery [29]. Several studies have reported abnormal microRNA production in urinary exosomes linked to various kidney diseases [30, 31], including a significant elevation of exosomal *miR-223-3p* in patients with CaOx kidney stones compared to healthy controls [32]. However, these studies often have small sample sizes, and a comprehensive microRNA signature in urinary exosomes specific to kidney stone patients remains insufficiently characterized.

The profile of urinary exosomal microRNA was assessed in a substantial cohort of kidney stone patients using Illumina BSB technology, supplemented by RT-qPCR for validation. Results identified four urinary exosomal microRNAs consistently elevated in patients, showing associations with distinct urinary compositions indicative of metabolic disruptions typical of kidney stones. Although the precise upstream signals triggering the elevation of these microRNAs remain unclear, the findings suggest active roles in disease pathogenesis rather than mere epiphenomena. Among these microRNAs, *miR-148b-5p* was particularly notable for enhancing urinary calcium excretion and facilitating kidney stone formation in hypercalciuria rat models, highlighting its potential as a therapeutic target for preventing calcium-containing kidney stones.

Besides *miR-148b-5p*, the other three microRNAs (*miR-31-5p, miR-205-5p*, and *miR-574-5p*) may also contribute to kidney stone formation, though their mechanisms of action remain unclear. Research suggests that *miR-31-5p* and *miR-574-5p* are involved in inflammation and apoptosis, which could influence kidney stone formation and progression [33, 34]. Moreover, *miR-205-5p* has been shown to inhibit MAGI1, mitigating injury in diabetic nephropathy, a condition linked to various renal dysfunctions [35].

Calcitonin, a key hormone in calcium metabolism, enhances calcium reabsorption and reduces phosphate reabsorption in renal tubules through its interaction with *Calcr* [36, 37]. It also facilitates renal reabsorption of both calcium and magnesium [38]. Calcr, a seven-transmembrane G-protein coupled receptor, is primarily expressed on epithelial cells in various nephron segments, including the thick ascending limb of the loop of Henlé, distal convoluted tubules, and collecting ducts [39, 40]. Notably, research has identified a strong association between single nucleotide polymorphisms (SNPs) in the *Calcr* gene and kidney stone formation, suggesting a role for *Calcr* in the pathogenesis of idiopathic hypercalciuria [41]. However, the influence of *Calcr* on urinary calcium excretion and kidney stone development remains under-documented. To address this gap, renal tubule-specific *Calcr* knockout mice were used to evaluate Calcr's role *Calcr* in urinary calcium excretion and the formation of calcium-containing kidney stones. The results demonstrated no increase in urinary calcium excretion in *Calcr* knockout mice on a normal diet. However, a calcium-rich diet resulted in a significant rise in urinary calcium excretion and the presence of CaOx crystals in the renal papillae. These data suggest that *Calcr* deficiency does not influence kidney stone development under normal dietary conditions but is crucial for calcium regulation and kidney stone susceptibility under high-calcium dietary conditions. This research highlights the importance of *Calcr* in renal calcium handling and is the first to demonstrate its specific role in the pathogenesis of calcium-containing kidney stones.

The precise mechanism through which renal *Calcr* reduces urinary calcium excretion remains unclear. It is hypothesized that calcitonin binding to its receptor enhances calcium reabsorption in the kidneys, thus decreasing urinary calcium excretion. This process does not appear to involve changes in TRPV5 or CaBP-D28K [42].

Recent advances in RNA biology have identified circRNAs as significant players in cellular regulation, demonstrated by their potential functions, regulatory networks, and

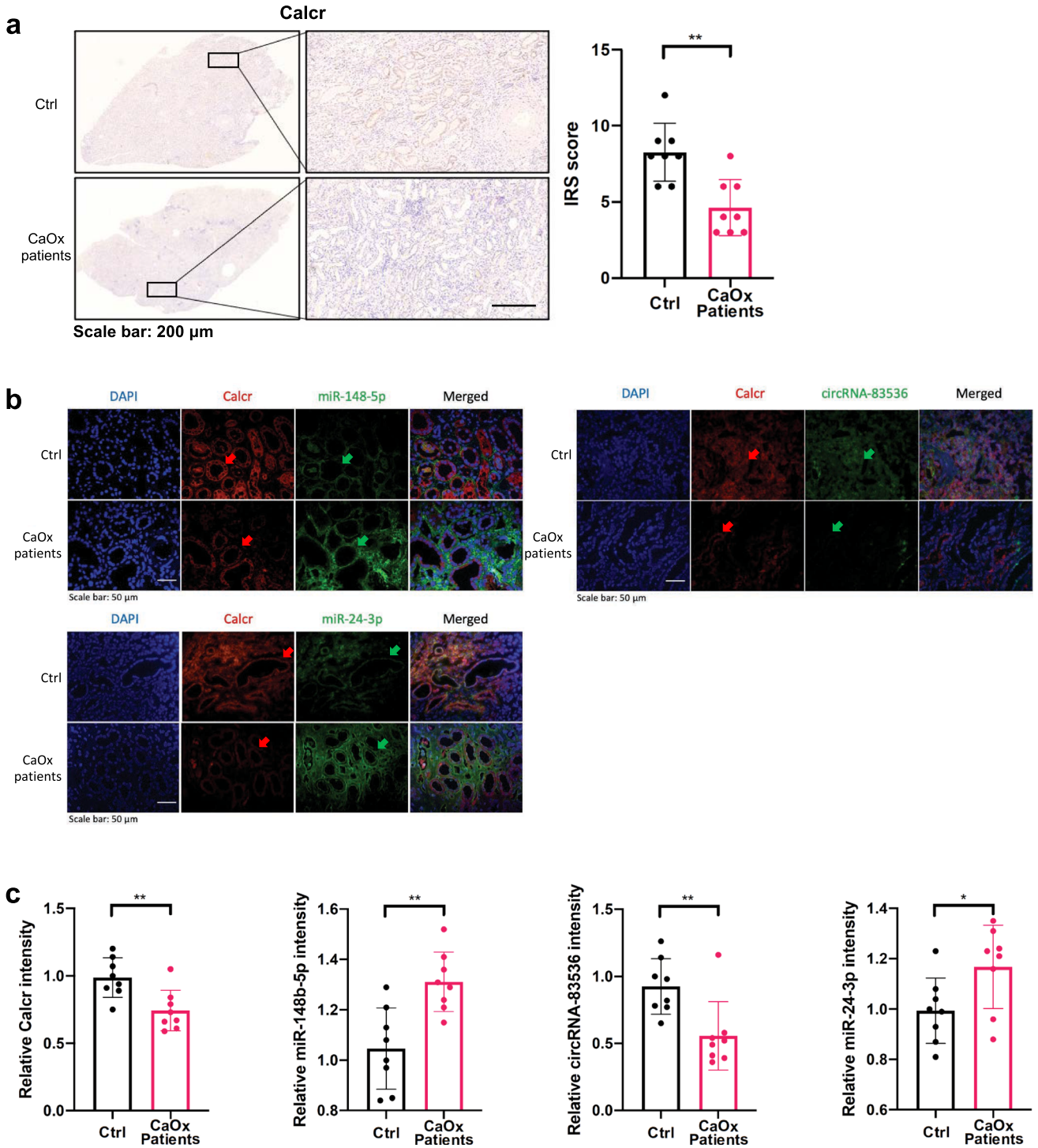

Fig. 8 Association of *miR-148b-5p*, *miR-24-3p*, *circRNA-83536,* and *Calcr* expression with kidney stones in human kidney tissues. **a** IHC staining of *Calcr* in kidney tissues from non-stone formers and kidney stone patients. **b** Representative FISH and IF images detecting *miR-148b-5p* (green arrows), *circRNA-83536* (green arrows), *miR-24-3p* (green arrows), and *Calcr* (red arrows) expression in kidney tissues from non-stone formers and kidney stone patients. Data are presented as mean ± SD from 8 samples per group. n.s indicates not significant; $^{*}P < 0.05$, $^{**}P < 0.01$ (Student's t-test)

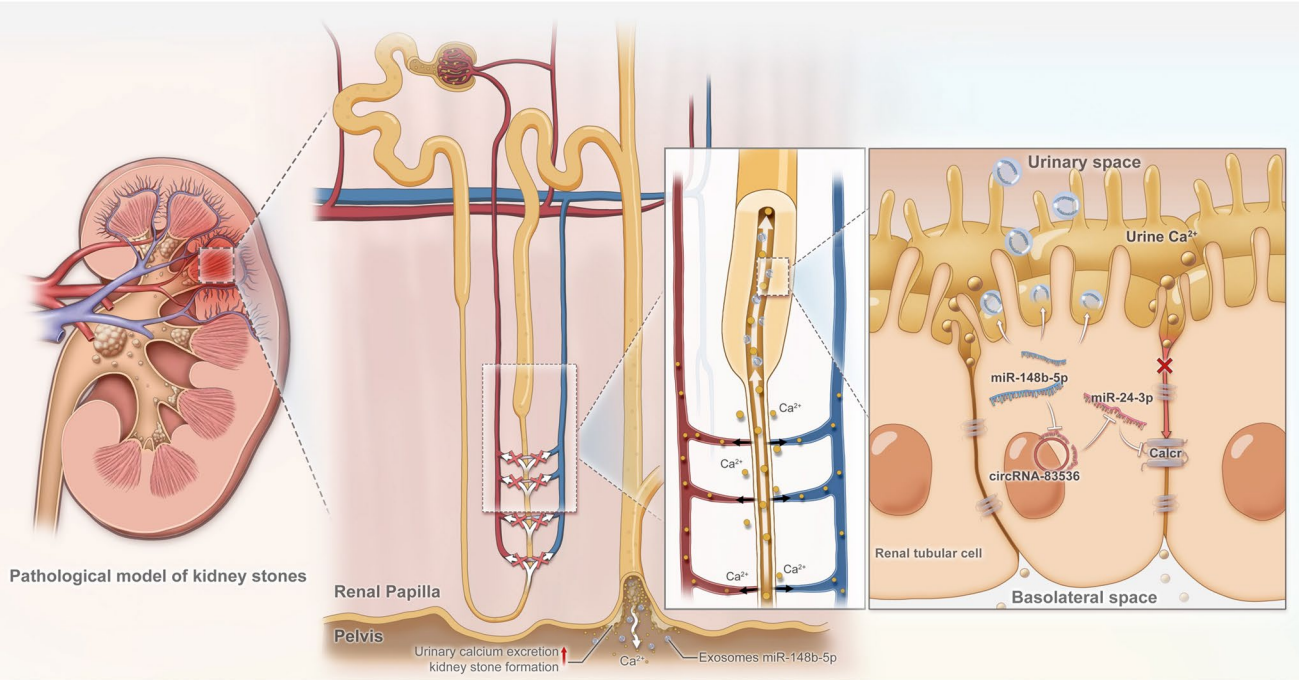

Fig. 9 Schematic representation of the *miR-148b-5p* regulatory pathway in kidney stone formation. The diagram depicts how *miR-148b-5p* inhibits *Calcr* expression via the *circRNA-83536/miR-24-3p* signaling axis, leading to elevated urinary calcium excretion and promoting kidney stone development

roles across various cell types and pathological states [43, 44]. These roles include microRNA sponging, gene splicing, transcriptional regulation, and modification of parental gene expression [45, 46]. Despite significant implications, circRNAs' roles in kidney stone disease remain underexplored, with literature largely confined to a single study examining circRNA profiles in an ethylene glycol-induced hyperoxaluria rat model [47]. The potential influence of circRNAs on kidney stone pathogenesis and their mechanisms is still mostly conjectural. No direct microRNA-responsive matches for *miR-148b-5p* seed sequences were identified in the 3'UTR of the *Calcr* gene, which led to the investigation of circRNAs as potential regulatory mediators. Results demonstrated that *miR-148b-5p* inhibited *circRNA-83536*, mitigating its suppression of *miR-24-3p*, and subsequently reducing *Calcr* expression. This novel circRNA-mediated regulatory pathway presents a promising therapeutic target for the prevention of calcium-containing stone formation.

This study has several limitations requiring further investigation. Firstly, while *miR-148b-5p* expression was found to be elevated in the urinary exosomes of kidney stone patients and its specific mechanism in influencing kidney stone formation was identified, the reason for this elevation was not explored. Additionally, although Calcr was identified as a necessary downstream effector for *miR-148b-5p*, the possibility that *miR-148b-5p* may impact kidney stone formation through other target genes or signaling pathways cannot be ruled out. Furthermore, the study focused on up-regulated microRNAs in exosomes, considering that inhibiting microRNA expression is generally more feasible for experimentation and clinical translation than overexpressing microRNAs. Future research must investigate the role of down-regulated microRNAs in kidney stone formation.

Conclusions

In conclusion, the present findings demonstrate that *miR-148b-5p* enhances urinary calcium excretion and contributes to the formation of calcium-containing kidney stones via the *circRNA-83536/miR-24-3p/*Calcr signaling pathway. Targeting this newly identified pathway offers potential for developing novel therapies to effectively suppress the formation and recurrence of calcium-containing kidney stones.

Supplementary Information The online version contains supplementary material available at https://doi.org/10.1007/s00018-024-05408-8.

Acknowledgements This research was funded by grants from the National Natural Science Foundation of China [grant numbers 82070721 and 82270822], the Guangdong Natural Science Foundation [grant number 2024A1515011644], and the Guangzhou Science Technology and Innovation Commission [grant numbers 2023A04J0574]. Acknowledgment is extended to EditChecks (https://editchecks.com.cn/) for providing linguistic assistance during the manuscript preparation.

Author contributions Guohua Zeng had full access to all study data and is responsible for the data integrity and accuracy of the data analysis. Study concept and design: Guohua Zeng and Yin Sun. Acquisition of data: Wei Zhu, Zhen Zhou, Chengjie Wu, Zhicong Huang, Ruiyue Zhao, Xinlu Wang, Lianmin Luo, Yang Liu, Wen Zhong, Zhijian Zhao, Guoyao Ai, Jian Zhong, Shusheng Liu, Weijie Liu, Xuliang Pang. Analysis and interpretation of data: Wei Zhu, Zhen Zhou, Chengjie Wu, Zhicong Huang. Drafting of the manuscript: Wei Zhu, Guohua Zeng. Critical revision of the manuscript for important intellectual content: Yin Sun. Statistical analysis: Wei Zhu, Zhen Zhou, Chengjie Wu, Zhicong Huang. Obtaining funding: Guohua Zeng, Wei Zhu. Administrative, technical, or material support: Lianmin Luo, Guoyao Ai. Supervision: Guohua Zeng. Other: None.

Funding National Natural Science Foundation of China,82070721,Guohua Zeng,82270822,Wei Zhu, Natural Science Foundation of Guangdong Province,2024A1515011644, Wei Zhu,the Guangzhou Science Technology and Innovation Commission, 2023A04J0574, Wei Zhu.

Data availability Exosome-microRNA-seq, RIP-seq, and additional relevant datasets supporting this study's conclusions are deposited in GEO under accession codes GSE241241, GSE241242, and GSE241243. These datasets will be accessible following the article's publication.

Declarations

Conflict of interest The authors declare no conflict of interest that could compromise the impartiality of the reported research.

Ethical approval This study was performed as per the principles of the Declaration of Helsinki and received approval from the Ethics Committee of the First Affiliated Hospital of Guangzhou Medical University (Date 2019/9/2).

Informed consent Informed consent was obtained from all participants.

Consent for publication Not applicable.

References

1. Scales CD, Smith AC, Hanley JM, Saigal CS (2012) Prevalence of kidney stones in the United States. Eur Urol 62:160–165
2. Zeng G, Mai Z, Xia S et al (2017) Prevalence of kidney stones in China: an ultrasonography based cross-sectional study. BJU Int 120:109–116
3. Zhu W, Liu Y, Lan Y et al (2019) Dietary vinegar prevents kidney stone recurrence via epigenetic regulations. EBioMedicine 45:231–250
4. Moe OW (2006) Kidney stones: pathophysiology and medical management. The Lancet 367:333–344
5. Pak CY (1998) Kidney stones. The Lancet 351:1797–1801
6. Curry JN, Saurette M, Askari M et al (2020) Claudin-2 deficiency associates with hypercalciuria in mice and human kidney stone disease. J Clin Invest 130:1948–1960
7. Evan A, Lingeman J, Coe FL, Worcester E (2006) Randall's plaque: pathogenesis and role in calcium oxalate nephrolithiasis. Kidney Int 69:1313–1318
8. Evan AP (2010) Physiopathology and etiology of stone formation in the kidney and the urinary tract. Pediatr Nephrol 25:831–841
9. Gong Y, Renigunta V, Himmerkus N et al (2012) Claudin-14 regulates renal Ca^{++} transport in response to CaSR signalling via a novel microRNA pathway. EMBO J 31:1999–2012
10. Gong Y, Himmerkus N, Plain A, Bleich M, Hou J (2015) Epigenetic regulation of MicroRNAs controlling CLDN14 expression as a mechanism for renal calcium handling. J Am Soc Nephrol 26:663–676
11. Kuo RL, Lingeman JE, Evan AP et al (2003) Endoscopic renal papillary biopsies: a tissue retrieval technique for histological studies in patients with nephrolithiasis. J Urol 170:2186–2189
12. Taguchi K, Usawachintachit M, Hamamoto S et al (2017) Optimizing RNA extraction of renal papilla biopsy tissue in kidney stone formers: a new methodology for genomic study. J Endourol 31:922–929
13. Mori MA, Ludwig RG, Garcia-Martin R, Brandão BB, Kahn CR (2019) Extracellular miRNAs: from biomarkers to mediators of physiology and disease. Cell Metab 30:656–673
14. Turchinovich A, Weiz L, Burwinkel B (2012) Extracellular miRNAs: the mystery of their origin and function. Trends Biochem Sci 37:460–465
15. Chen T, Wang C, Yu H et al (2019) Increased urinary exosomal microRNAs in children with idiopathic nephrotic syndrome. EBioMedicine 39:552–561
16. Min Q-H, Chen X-M, Zou Y-Q et al (2018) Differential expression of urinary exosomal microRNAs in IgA nephropathy. J Clin Lab Anal. https://doi.org/10.1002/jcla.22226

17. Letavernier E, Verrier C, Goussard F et al (2016) Calcium and vitamin D have a synergistic role in a rat model of kidney stone disease. Kidney Int 90:809–817
18. Shao X, Somlo S, Igarashi P (2002) Epithelial-specific Cre/lox recombination in the developing kidney and genitourinary tract. JASN 13:1837–1846
19. Pizzolato P (1964) Histochemical recognition of calcium oxalate. J Histochem Cytochem 12:333–336
20. Remmele W (1987) Stegner HE [recommendation for uniform definition of an immunoreactive score (IRS) for immunohistochemical estrogen receptor detection (ER–ICA) in breast cancer tissue]. Pathologe 8:138–140
21 Andreu Z, Yáñez-Mó M (2014) Tetraspanins in extracellular vesicle formation and function. Front Immunol. https://doi.org/10.3389/fimmu.2014.00442
22. Geekiyanage H, Rayatpisheh S, Wohlschlegel JA, Brown R, Ambros V (2020) Extracellular microRNAs in human circulation are associated with miRISC complexes that are accessible to anti-AGO2 antibody and can bind target mimic oligonucleotides. Proc Natl Acad Sci 117:24213–24223
23. Panda AC (2018) Circular RNAs act as miRNA sponges. Adv Exp Med Biol 1087:67–79
24. Loher P, Rigoutsos I (2012) Interactive exploration of RNA22 microRNA target predictions. Bioinformatics 28:3322–3323
25. Dudekula DB, Panda AC, Grammatikakis I, De S, Abdelmohsen K, Gorospe M (2016) CircInteractome: a web tool for exploring circular RNAs and their interacting proteins and microRNAs. RNA Biol 13:34–42
26. Wu W, Ji P, Zhao F (2020) CircAtlas: an integrated resource of one million highly accurate circular RNAs from 1070 vertebrate transcriptomes. Genome Biol 21:101
27. Hansen TB, Jensen TI, Clausen BH et al (2013) Natural RNA circles function as efficient microRNA sponges. Nature 495:384–388
28. van Balkom BWM, Pisitkun T, Verhaar MC, Knepper MA (2011) Exosomes and the kidney: prospects for diagnosis and therapy of renal diseases. Kidney Int 80:1138–1145
29. Shin S, Park YH, Jung S-H et al (2021) Urinary exosome microRNA signatures as a noninvasive prognostic biomarker for prostate cancer. NPJ Genom Med 6:45
30. Sun IO, Lerman LO (2019) Urinary microRNA in kidney disease: utility and roles. Am J Physiol-Ren Physio 316:F785–F793
31. Magayr TA, Song X, Streets AJ et al (2020) Global microRNA profiling in human urinary exosomes reveals novel disease biomarkers and cellular pathways for autosomal dominant polycystic kidney disease. Kidney Int 98:420–435
32. Yang Y, Wang Q, Xun Y, Li C, Wang S (2022) The preliminary exploration of what role miRNAs derived from urinary exosomes play in kidney stone formation. Urology 166:104–110
33. Hegewald AB, Breitwieser K, Ottinger SM et al (2020) Extracellular miR-574-5p induces osteoclast differentiation via TLR 7/8 in rheumatoid arthritis. Front Immunol. https://doi.org/10.3389/fimmu.2020.585282
34. Kim S, Lee K-S, Choi S et al (2018) NF-κB–responsive miRNA-31-5p elicits endothelial dysfunction associated with preeclampsia via down-regulation of endothelial nitric-oxide synthase. J Biol Chem 293:18989–19000
35. Xiang Y, Sun M, Wu Y, Hu Y (2024) MiR-205-5p-mediated MAGI1 inhibition attenuates the injury induced by diabetic nephropathy. Pharmacology 109:98–109
36. Carney SL (1997) Calcitonin and human renal calcium and electrolyte transport. Miner Electrolyte Metab 23:43–47
37. Hsu Y-J, Dimke H, Hoenderop JGJ, Bindels RJM (2010) Calcitonin-stimulated renal Ca^{2+} reabsorption occurs independently of TRPV5. Nephrol Dial Transplant 25:1428–1435
38. Carney S, Thompson L (1981) Acute effect of calcitonin on rat renal electrolyte transport. Am J Physiol-Ren Physiol 240:F12–F16
39. Masi L, Brandi ML (2007) Calcitonin and calcitonin receptors. Clin Cases Miner Bone Metab 4:117–122
40. Ali FT, El-Azeem EMA, Hekal HFA et al (2022) Association of TRPV5, CASR, and CALCR genetic variants with kidney stone disease susceptibility in Egyptians through main effects and gene–gene interactions. Urolithiasis 50:701–710
41. Chen WC, Wu HC, Lu HF, Chen HY, Tsai FJ (2001) Calcitonin receptor gene polymorphism: a possible genetic marker for patients with calcium oxalate stones. Eur Urol 39:716–719
42. Moor MB, Bonny O (2016) Ways of calcium reabsorption in the kidney. Am J Physiol-Ren Physiol 310:F1337–F1350
43. Pamudurti NR, Bartok O, Jens M et al (2017) Translation of CircRNAs. Mol Cell 66:9-21.e7
44. Meng S, Zhou H, Feng Z et al (2017) CircRNA: functions and properties of a novel potential biomarker for cancer. Mol Cancer 16:94
45. Kristensen LS, Jakobsen T, Hager H, Kjems J (2022) The emerging roles of circRNAs in cancer and oncology. Nat Rev Clin Oncol 19:188–206
46. Chen L-L (2020) The expanding regulatory mechanisms and cellular functions of circular RNAs. Nat Rev Mol Cell Biol 21:475–490
47. Cao Y, Gao X, Yang Y, Ye Z, Wang E, Dong Z (2018) Changing expression profiles of long non-coding RNAs, mRNAs and circular RNAs in ethylene glycol-induced kidney calculi rats. BMC Genomics 19:660